chemosensors

MDPI

Review

Chemical Sensing and Analysis with Optical Nanostructures

Chenyu Dong, Yifan Wang, Xiaoyan Zhao, Jie Bian and Weihua Zhang *

College of Engineering and Applied Sciences, State Key Laboratory of Analytical Chemistry for Life Science, and Jiangsu Key Laboratory of Artificial Functional Materials, Nanjing University, Nanjing 210023, China
* Correspondence: zwh@nju.edu.cn

Abstract: Nanostructures and nanomaterials, especially plasmonic nanostructures, often show optical properties that conventional materials lack and can manipulate light, as well as various light–matter interactions, in both their near-field and far-field regions with a high efficiency. Thanks to these unique properties, not only can they be used to enhance the sensitivity of chemical sensing and analysis techniques, but they also provide a solution for designing new sensing devices and simplifying the design of analytical instruments. The earliest applications of optical nanostructures are surface-enhanced spectroscopies. With the help of the resonance field enhancement of plasmonic nanostructures, molecular signals, such as Raman, infrared absorption, and fluorescence can be significantly enhanced, and even single-molecule analysis can be realized. Moreover, the resonant field enhancements of plasmonic nanostructures are often associated with other effects, such as optical forces, resonance shifts, and photothermal effects. Using these properties, label-free plasmonic sensors, nano-optical tweezers, and plasmonic matrix-assisted laser desorption/ionization have also been demonstrated in the past two decades. In the last few years, the research on optical nanostructures has gradually expanded to non-periodic 2D array structures, namely metasurfaces. With the help of metasurfaces, light can be arbitrarily manipulated, leading to many new possibilities for developing miniaturized integrated intelligent sensing and analysis systems. In this review, we discuss the applications of optical nanostructures in chemical sensing and analysis from both theoretical and practical aspects, aiming at a concise and unified framework for this field.

Keywords: optical nanostructure; plasmonics; surface-enhanced spectroscopy; sensing; miniaturization

Citation: Dong, C.; Wang, Y.; Zhao, X.; Bian, J.; Zhang, W. Chemical Sensing and Analysis with Optical Nanostructures. *Chemosensors* **2023**, *11*, 497. https://doi.org/10.3390/chemosensors11090497

Academic Editor: Marco Pisco

Received: 25 June 2023
Revised: 4 September 2023
Accepted: 7 September 2023
Published: 9 September 2023

1. Introduction

Scientists have long dreamed of a rapid, simple, and low-cost analytical technique for tracing amounts of components in complex samples. This technique has broad applications in chemistry, material sciences, and life sciences but also presents a great challenge to researchers. Traditional methods are no longer applicable when faced with very small quantities of molecules or samples with complex nanostructures and nano-compositions (such as single cells, a droplet of blood, and complex polymer mixtures) due to the limitations of sample size and scale. New physical or chemical effects are required to transduce and amplify extremely weak sample information into readable physical signals. To meet this demand, many new advanced analytical techniques, particularly optical methods, have been developed in the last few decades thanks to breakthroughs in nano-optics.

Optical techniques are the most widely used techniques in chemical sensing and analysis because light–matter interactions are one of the most fundamental types of physical interactions in nature and form the basis of many analytical methods [1,2]. For example, the optical interactions with molecules' electronic states lead to UV-Vis spectroscopy, and interactions with the vibrational states lead to Raman spectroscopy and infrared spectroscopy. Using the optothermal effect, one can even vaporize and ionize molecules and subsequently measure their molecular weights. At the same time, with the development of the semiconductor industry, crucial components, e.g., lasers and photodetectors, have become cheap and easy to access today. All these factors have made optics a powerful,

versatile, and convenient choice for chemical sensing and analysis. However, light–matter interactions are generally weak due to the fact that the size of molecules is several orders of magnitude smaller than the wavelength of light. This causes the sensitivity issue in optical measurements (Figure 1). Fortunately, the development of nano-optical technology makes it possible to circumvent this issue and obtain ultrasensitive analysis [3–5]. With an optical nanostructure, light can be resonantly enhanced, scattered, and absorbed, and one can therefore enhance local optical signals significantly, making ultrasensitive nano-analysis possible [6–8].

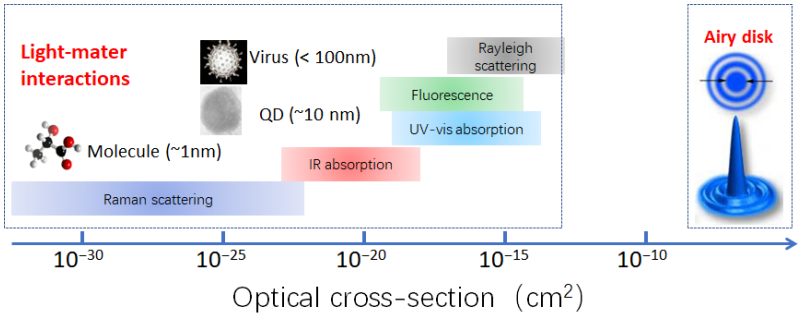

Figure 1. Optical cross-sections of typical light–matter interactions at the nanoscale.

To date, countless optical nanostructures, particularly metallic nanostructures, with different shapes and properties have been studied. The metallic nanostructures are also known as plasmonic nanostructures because they support collective oscillations of electrons (so-called plasmon polaritons). These plasmon oscillations can be divided into two categories: (1) surface plasmon resonance (SPR), which propagates along the surface of metal surfaces, and (2) localized surface plasmon resonance (LSPR), which cannot [9–11]. Both are tightly confined at the surfaces of structures and, in particular, with LSPR, light can be confined to sub-10 nm "hot spots" adjacent to metal nanostructures. This extreme light confinement can also lead to strong local enhancement of the electric fields and consequently various light–matter interactions, making it very useful in various analysis techniques (Figure 2). For example, when a molecule is placed in a "hot spot", its signal (e.g., Raman scattering, fluorescence, and absorption) can be increased by several orders of magnitude, and even single-molecule Raman detection can be achieved [12,13]. The presence of the molecule also shifts the plasmon resonance, and in other words, the plasmonic nanostructure can also be used as a high-performance index nanosensor [14–17]. Moreover, thanks to their strong optothermal effects, plasmonic nanostructures can even be used as the ion source for mass spectrometry (MS) [18–20]. Besides the plasmonic structure, it was reported that dielectric micro-resonators can also be used for detecting chemicals or viruses by monitoring the induced resonance shifts, which is similar to the LSPR sensors [21–25]. However, due to the absence of free electrons, these dielectric micro-resonators cannot confine or absorb light like their metallic counterparts.

In recent years, researchers started to realize that one can achieve arbitrary regulation of the wavefront of light by patterning separated nanostructures into a planar 2D device, which is also known as a metasurface [26,27]. A variety of designs have been demonstrated, including periodic arrays, gradient structures, and even more complex designs. With these structures, one can conduct sensing, imaging, spectroscopy, and even polarimetry with good quality and efficiency [28–35]. This not only opens the door towards new sensor designs but also makes the miniaturization of conventional analysis equipment possible.

Today, optical nanostructures have become one of the most dynamic research areas in chemical sensing and analysis, and there have been quite a few review articles on this topic [36–38]. Most of them are mainly focused on the applications related to field confinement and enhancement, such as surface-enhanced spectroscopies and LSPR-based sensors, but other important topics, such as photothermal effect-related applications, miniaturized sensors, and metasurface-based polarimetric techniques, are not covered. We, therefore,

write this review to sort out the various basic properties of nano-optical structures, further discuss their applications in chemical analysis, from conventional surface-enhanced spectroscopies and index sensing to more complex phenomena like laser-induced desorption and ionization, and then cover the application of metasurfaces for circular dichroism (CD) measurement, as shown in Figure 2.

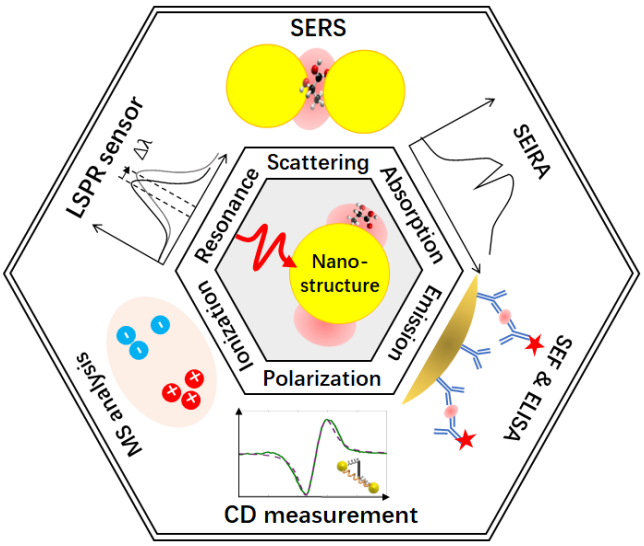

Figure 2. Chemical sensing and analysis with optical nanostructures.

2. Optical Properties of Nanostructures

In this section, we will give a concise review of the theory of the localized plasmon resonance of subwavelength nanostructures. Associated optical effects, such as field confinement, field enhancement, and local heating, which are crucial for chemical sensing and analysis, will also be discussed. At the end of this section, some of the basic ideas of metasurfaces will also be introduced based on the discussion of the local behaviors of subwavelength optical nanostructures.

2.1. Localized Plasmon Resonance and Field Enhancement

The simplest model for understanding plasmon resonance phenomena is spherical nanoparticles [11]. When the nanoparticle's size is much smaller than the wavelength of light, it can be treated as a dipole,

$$\mathbf{p} = \varepsilon_0 \alpha \mathbf{E}. \tag{1}$$

Here, α is the polarizability, and $\mathbf{E}$ is the external excitation field. The light scattering cross-section and absorption cross-section of this structure then become:

$$\mathrm{A}_{sca} = \frac{k^4}{6\pi}|\alpha|^2 \tag{2}$$

$$\mathrm{A}_{abs} = kIm(\alpha) \tag{3}$$

For a deep subwavelength particle, α has a simple form:

$$\alpha = 4\pi r^3 \frac{\varepsilon - \varepsilon_0}{\varepsilon + 2\varepsilon_0} \tag{4}$$

Interestingly, for metallic materials, the real part of the ε is negative when the frequency is below their bulk plasma resonance frequencies, which typically lie within the optical spectral range. As a result, the denominator of the α can approach zero, resulting in a

strong resonance of the free electrons (i.e., localized plasmon resonances). This leads to the strong scattering and absorption of light by the nanostructures.

The above plasmon resonances are not limited to spherical particles and can occur for any metallic nanoparticles with any shape [39,40]. Theoretically, the scattering problem of electromagnetic fields can be rigorously described and solved using the Lippmann–Schwinger equation [41]:

$$\boldsymbol{E}(\boldsymbol{r}) = \boldsymbol{E}_{ext}(\boldsymbol{r}) + \int_{cavity} d\boldsymbol{r}' \boldsymbol{G}_0(\boldsymbol{r}, \boldsymbol{r}') \cdot \Delta\varepsilon(\boldsymbol{r}') k_0{}^2 \boldsymbol{E}(\boldsymbol{r}') \tag{5}$$

where $\Delta\varepsilon = \varepsilon_c - \varepsilon_0$ is the permittivity contrast between the scatter (nanocavity in this work) and the background medium, E_{ext} is the external field, G_0 is the free-space Green's tensor, and k_0 is the wavenumber in the background medium. In previous works, the author of this work demonstrated that under the quasi-static approximation, a nanoparticle always has a complete set of orthogonal eigenmodes, $|\boldsymbol{E}_i\rangle$. The scattering fields E, obtained under excitation field E_0, can be written as a linear superposition of this set of eigenmodes (Figure 3):

$$\mathbf{E} = \sum_i a_i \mathbf{E}_i \tag{6}$$

$$\boldsymbol{a_i} = \frac{\boldsymbol{s}}{\boldsymbol{s} - \boldsymbol{s_i}} \langle \mathbf{E}_i | \mathbf{E}_0 \rangle \tag{7}$$

Here, $s = \varepsilon_0/(\varepsilon_c - \varepsilon_0)$ is a material-related parameter, and s_i are the eigenvalues.

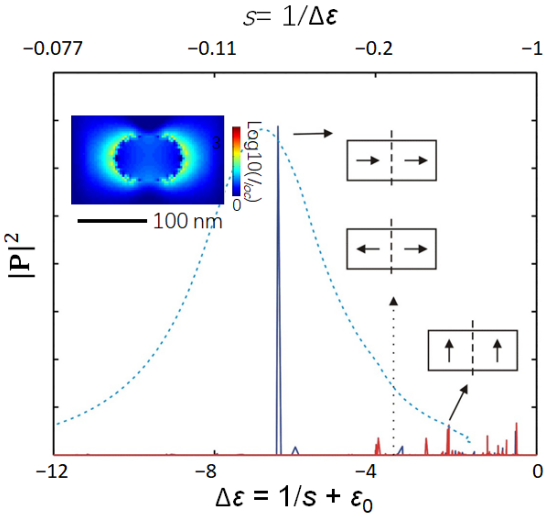

Figure 3. Eigenmodes of a plasmonic nanostructure. The arrows depict the symmetry of the eigenmodes. Inset is the field distribution of the dominant dipole mode.

Equation 5 can be numerically used after being discretized, and interestingly, it can be shown that s_i are always between -1 and 0 [41]. Considering that the permittivity of the local environment, ε_0, is positive (e.g., $\varepsilon_0 = 1$ for vacuum), it means that a negative permittivity is always required to reach the resonance condition of a subwavelength nanostructure. In the optical regime, only metals exhibit negative dielectric constants due to the existence of free electrons [8]. This explains why only metal nanostructures show extraordinary optical properties in the optical regime.

In the quasi-electrostatic model described above, the field enhancement effect is determined by two factors, (1) resonance enhancement and (2) mode distribution, that is, the field distribution of the eigenmode $|\mathbf{E}_i\rangle$. The first factor is determined by the intrinsic properties of the material. At the resonance wavelength, the real part of the denominator of $s/(s - s_i)$ will be zero, and it is evident that the smaller the imaginary part of the dielectric

constant of the material is, the greater the resonance enhancement will be. For noble metals, e.g., Ag and Au, the resonance factors can be greater than ten or even reach hundreds. The second factor is determined by the geometry of the nanostructure. It is well known that large field enhancement is often associated with some specific features, such as sharp corners (i.e., lightning rod effect) and nanometer gaps [42]. In practice, by combining both the resonance and geometric effects, the field enhancement factor, $g = |\mathbf{E}| / |\mathbf{E}_0|$, can reach >100 times at some "hot spots". If there are molecules present in the "hot spot", their excitation rate will be increased by a factor of g^2, which is more than 10,000 times.

The above theoretical description can also be understood with the following physical picture. At the resonance frequency, a plasmon nanostructure can collect propagating light in free space from a cross-section larger than its geometric size and squeeze the light into nanometer "hot spots". This process is very similar to the function of radio antennas, which can collect the radio waves in the free space into their near field efficiently. This is why plasmon nanostructures are often called optical antennas or plasmonic nano-antennas [43–45].

2.2. Enhancement of the Near-Field Scattering and Fluorescence Emission

In antenna theory, it is known that radio antennas are bidirectional devices. They not only collect the far-field signals to their near field but also broadcast signals from their near-field to the far-field region [46]. Similarly, plasmon nanostructures can also greatly increase the rate of Raman scattering, as well as the fluorescence radiation of molecules in their near-field range. The former can be understood using the reciprocity principle in light scattering, and to understand the latter, one needs to consider the change in the local density of states caused by the antenna.

Let us first examine the process of Raman scattering. We consider a molecule located at $\mathbf{r}_1$ in the near field of a metallic particle, and the scattered signal $\mathbf{E}$ at $\mathbf{r}_2$ in the far field can then be described using Green's function $\mathbf{G}(\mathbf{r}_2, \mathbf{r}_1)$, as shown in Figure 4a. To excite the Raman signal, we let the emission of a dipole at $\mathbf{r}_2$ be the incident light, and at $\mathbf{r}_1$, the local excitation can be described by $\mathbf{G}(\mathbf{r}_1, \mathbf{r}_2)$, as shown in Figure 4b. In most cases, the reciprocal principle holds [46,47]:

$$\mathbf{G}(\mathbf{r}_1, \mathbf{r}_2) = \mathbf{G}(\mathbf{r}_2, \mathbf{r}_1) \tag{8}$$

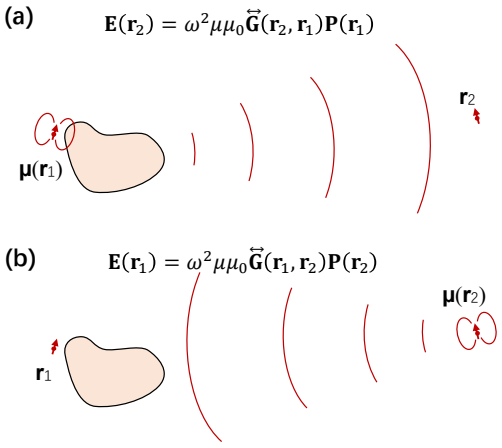

Figure 4. Reciprocity in light scattering. (**a**) The scattered signal $\mathbf{E}$ at $\mathbf{r}_2$ in the far field can be described using Green's function $\mathbf{G}(\mathbf{r}_2, \mathbf{r}_1)$. (**b**) The local excitation at $\mathbf{r}_1$ can be described by $\mathbf{G}(\mathbf{r}_1, \mathbf{r}_2)$.

In other words, if exaction light is enhanced by g^2 times due to the presence of the particle, in the emission process from $\mathbf{r}_1$ to $\mathbf{r}_2$, the signal will be enhanced by g^2 times again. Therefore, the total enhancement of the Raman signal is g^4, which is called the fourth power law in surface-enhanced Raman spectroscopy.

On the other hand, the enhancement of the emission process of fluorescence is very different because it is linked with the change in the lifetime of the electronic states, which can no longer be described by the theory of classical electrodynamics. To describe the emission process, Fermi's Golden Rule is used [3,6]. That is, the rate of transition (radiation) of molecules is completely determined by the local density of state (LDOS), ρ:

$$\gamma_{i-f} = \frac{2\pi}{\hbar}\left|\langle f|H'|i\rangle\right|^2 \rho(E_f) \tag{9}$$

Interestingly, although state density is a quantum concept, it can be derived from the Green's function, which describes the classical electromagnetic fields [8,48,49], namely:

$$\rho(\mathbf{r},\omega) = \frac{2\omega}{\pi c^2} Im\{Tr[\mathbf{G}(\mathbf{r},\mathbf{r},\omega)]\} \tag{10}$$

When a plasmonic nanostructure is present, the LDOS can be significantly enhanced. This can be calculated using Equation (10), where Green's tensor can be directly calculated using iterative techniques developed by Martin and colleagues [50]. The LDOS can also be obtained using Equation (9), which states that the LDOS is proportional to the emission rate and, consequently, the power of a dipole source. One can therefore calculate the LDOS by simulating the emission properties of a dipole source using normal numerical solvers for electromagnetic fields, e.g., the finite-difference time-domain (FDTD) and finite element method (FEM).

Fluorescence signals can be affected by many factors, such as temperature, pH, concentration, and so on. In addition to the emission rate, the fluorescence signal can also be influenced by the quantum yield. The presence of plasmonic nanoparticles may lower the quantum yield due to the material losses of metal, and this can even quench the fluorescence signals despite the enhancement [51,52], particularly for the dye molecules in the visible spectral range, whose intrinsic quantum yields are often close to 100% [53].

It is also worth noting that surface-enhanced fluorescence (SEF) experiments are normally only performed with weak excitation light. When the excitation becomes strong, the excitation rate will reach the emission rate, and that will saturate the system. In this case, the local field enhancement will not influence the signal intensity anymore.

2.3. Plasmonic Trapping and Sensing

Another important effect related to the local field enhancement is the significant increase in the field gradient, which has been widely used for optical trapping and sensing in the last two decades. At a "hot spot", the intensity gradient of light can be enhanced by more than three orders of magnitude thanks to both the enhancement and spatial confinement of fields [54]. This will greatly enhance the gradient forces (also known as the dielectrophoresis effect in chemistry), leading to non-negligible attractions for nanoparticles and surrounding molecules. With the plasmon-enhanced trapping forces, individual nanoparticles and even biomolecules can be trapped under milliwatt-scale laser illumination, allowing researchers to enrich molecules at "hot spots" and investigate them further with surface-enhanced spectroscopy techniques [17,55,56].

Interestingly, if we treat the nanoparticle as an optical nano-resonator without radiation losses, we can link the trapping effect with the optical sensing techniques together. When a molecule or nanoparticle is trapped, the energy of the system will become lower, and consequently, the resonance frequency of the plasmonic nanostructure will be shifted. This property makes the plasmonic nanostructure a high-performance nanosensor that is extremely sensitive to external analytes [55]. Today, this effect has been widely used for label-free detections of local index changes induced by the analytes in the surrounding environment.

Using perturbation theory, the above resonance frequency change can be described with an explicit formula [57]:

$$\Delta\omega_i = -\alpha_{NP}\frac{d\omega_i}{d\varepsilon_{ca}}\frac{|\mathbf{E}(\mathbf{r}_{NP})|^2}{\int_{cavity} d\mathbf{r}|\mathbf{E}(\mathbf{r})|^2} \tag{11}$$

This is similar to the case of dielectric microcavities, whose resonance frequency shift can be written as:

$$\Delta\omega_i = -\frac{\omega_i}{2}\frac{\int d\mathbf{r}\Delta\varepsilon(\mathbf{r})|\mathbf{E}(\mathbf{r})|^2}{\int d\mathbf{r}\varepsilon(\mathbf{r})|\mathbf{E}(\mathbf{r})|^2} \tag{12}$$

In both cases, the resonance frequency shift is proportional to both the local light intensity and the refractive index change induced by the trapped nano-objects. Therefore, a larger enhancement will always lead to a better sensitivity of the LSPR-based sensors.

Meanwhile, there are also differences between Equations (11) and (12). In Equation (12), the resonance shift is inversely proportional to $\int d\mathbf{r}\varepsilon(\mathbf{r})|\mathbf{E}(\mathbf{r})|^2$, the integral of the electric field energy over the whole space, while in Equation (11), the integral is limited to the space inside the cavity. This is because, for the resonance mode of a plasmonic nanocavity, the integral $\int d\mathbf{r}\varepsilon(\mathbf{r})|\mathbf{E}(\mathbf{r})|^2 = 0$ is due to the negative permittivity of the metal.

2.4. Photothermal Effect

Large field enhancement means strong optical absorption. From Equation (3), it can be seen that the absorption cross-section of a nanoparticle can also be enhanced by resonance. In the case of gold and silver nanoparticles, their absorption interface can even be greater than their physical size. Meanwhile, the heat capacity and dissipation rate of plasmonic nanoparticles are often very low. For example, in the case of porous nanostructures where all nanopores are aligned along the z direction, the effective thermal capacity C_{eff} and conductivity along the z direction $K_{eff,zz}$ and x-y direction $K_{eff,xy}$ can be written as

$$C_{eff} = \phi C_1 + (1-\phi)C_2 \tag{13}$$

$$\frac{K_{eff,zz}}{K_m} = 1 + (\frac{K_1 - K_m}{K_m})\phi \tag{14}$$

$$\frac{K_{eff,xy}}{K_m} = 1 + \frac{2\phi}{A_1 - \phi + A_2(0.30584\phi^4 + 0.013363\phi^8)} \tag{15}$$

where C_1, C_m, K_1, and K_m are the thermal capacity and conductance of the filler and matrix, respectively, ϕ is the volume fraction of the filler, $A_1 = \frac{K_1+K_m}{K_1-K_m}$, and $A_2 = \frac{K_2+K_m}{K_2-K_m}$. Consider that the filler is air and its thermal capacity and conductivity are close to zero. When ϕ is close to 1, the thermal capacity and conductivity of the porous material will be very small. It is therefore possible to obtain unexpectedly high temperatures under a relatively mild excitation using specially designed plasmonic nanostructures [18]. This provides a new solution for energy-intensive processes, e.g., water desalination and sewage treatment [19]. In the chemical analysis, it has been demonstrated that the high temperature can be used to improve the efficiency of laser-induced desorption and ionization [58].

2.5. Metasurfaces and Light Manipulation

The plasmon resonance effect not only provides a means for the enhancement/regulation of the local field strength but also enables the manipulation of the local phase and polarization of the optical field [26,27]. In other words, it is possible to manipulate light arbitrarily at any point in space. Based on this idea, Capasso and coworkers proposed the concept of metasurfaces, which use arrays of plasmon nanostructures to regulate wavefronts at every point in space. This idea greatly expands the design freedom of optical devices

and provides a new path for the development of optical sensing devices and analytical instruments [31,32].

In light manipulation, precise control of phase is crucial. There are two main methods: resonance tuning and geometric phase. The former uses the resonance behavior of the optical nanostructure to tune the local phase of light [26]. By changing the resonance across the working frequency, one can adjust the phase of the scattered light, achieving a 180-degree phase shift. The method is simple and efficient but is wavelength-dependent and often causes undesired dispersions. Another method is the geometric phase [59–61]. We know that linearly polarized light is the superposition of left-handed and right-handed circular polarized components. After a simple calculation, one can find that the phase of the left and right circular polarization components is linearly related to the direction of the linearly polarized light. In other words, the phase of circularly polarized light can be controlled by simply manipulating the polarization direction of the field using anisotropic nanostructures. The method is solely determined by the geometric parameters of the nanostructure and is independent of wavelength but has relatively low conversion efficiency. In addition to the above methods, other phase control methods were also demonstrated, e.g., the waveguide method in dielectric metasurfaces. Using the above method, traditional bulky optical systems can be replaced with an ultra-thin planar structure. This opens up many new exciting possibilities for future instrument design [27].

3. Surface-Enhanced Spectroscopies

In this section, we will give a brief review of the surface-enhanced spectroscopies, which are direct applications of large field enhancement of plasmonic nanostructures. They are also the most important and widely studied topics in nanostructure-based chemical analysis.

3.1. Surface-Enhanced Raman Scattering

Raman spectroscopy is commonly known as the fingerprint of molecules in analytical chemistry, but Raman signals are commonly extremely weak, preventing them from being used in many applications. Because of this, SERS attracted a lot of attention after it was first reported in the 1970s [62–64]. In particular, Nie and Kneipp's groups independently reported single-molecule Raman measurements from some "hot spots" of Ag nanoparticles [12,13], and for the first time, people were capable of performing structural analysis for individual molecules in an ambient environment. Encouraged by this, many researchers carried out research over the last two decades to develop SERS into a quantitative, robust, and reliable ultrasensitive analytical method. However, it was found that SERS had a series of limitations due to its own mechanism [65].

One of the major challenges in SERS is the fabrication of high-performance SERS substrates, which is a long-standing issue in the field. In the early stages, SERS is often performed with rough metal surfaces or metallic nanoparticle aggregates, in which "hot spots" can be randomly formed in the nanogaps between particles (Figure 5a) [66]. Later, the concept of nano-antennas was introduced [43], and "hot spots" can be designed and fabricated using laterally coupled structures in a "controllable" fashion (Figure 5c) [43,67–69]. However, until around 2010, "hot spots" on SERS substrates were always sparse and random. This sparse random "hot spots" problem stems from the fact that the enhancement factor of a "hot spot" is extremely sensitive to its local geometry. The SERS performance can be very different even if two nanostructures are almost identical under electron microscopy. For example, one of the authors of this work demonstrated that even 1 nm surface roughness can lead to a one order of magnitude change in the Raman signal [70]. Moreover, nanometer features are unstable under illumination due to local photothermal effects [71]. It is therefore almost impossible to create "hot spots" in a repeatable fashion because it is extremely difficult to control the detailed features at the nanoscale using conventional nanofabrication techniques.

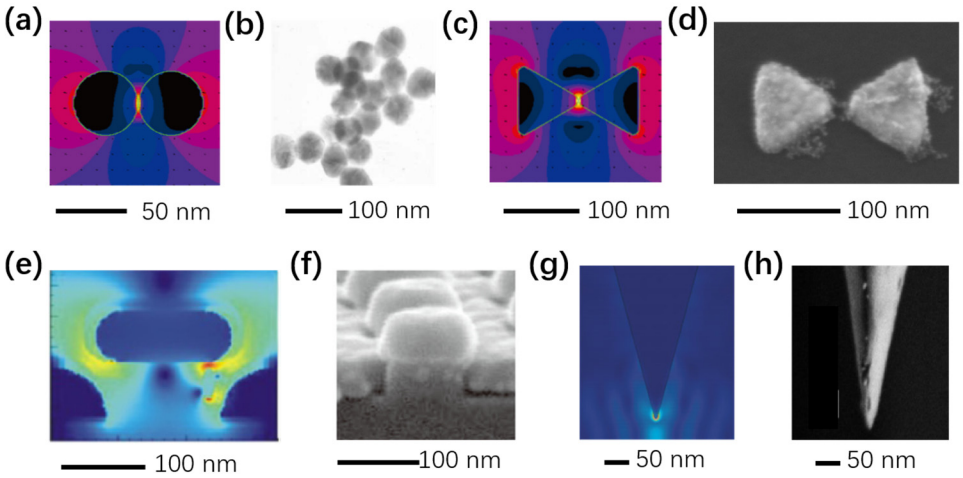

Figure 5. Different types of "hot spots" in surface-enhanced spectroscopies. (**a**,**b**) The field enhancement and SEM image of a nanoparticle cluster [72]. (**c**,**d**) Plasmonic bow-tie nano-antenna. (**e**,**f**) Vertically coupled plasmonic nanocavity array [73]. (**g**,**h**) Metallic nanotip [72].

To solve this problem, various vertically coupled designs were proposed to circumvent the fabrication challenge faced by laterally coupled structures (Figure 5e). Currently, deposition and etching techniques allow us to control the thickness of a layer at sub-nanometer precision. It is, therefore, possible to construct vertically coupled nanostructures with extremely high precision [74–76]. To date, various vertically coupled structures with a high density and large area uniformity of "hot spots" have been reported, and with these structures, SERS has gradually become a quantitative analytical tool [77].

Recently, some successful strategies that partly overcome this problem have been reported. One work reported that alkanethiolate ligand-regulated Ag nanoparticle films can be used to achieve quantitative SERS measurements down to the single-molecule level [78]. Another showed that arrays of weakly coupled Ag nanohelices achieved both homogeneous and strong near-field enhancements [79]. These works allow reproducible SERS detection over a large area with excellent uniformity and a high Raman enhancement factor.

Another challenge in SERS is that the SERS signals from "hot spots" are very unstable and often contaminated. The main reason is that the local metal structures of "hot spots" are very "active" due to the photothermal effect, as well as photocatalysis processes. To avoid the above problems, researchers have developed ultra-thin protective layer technology for SERS substrates, which greatly improves the stability of signals [80].

In addition to top-down microfabrication technology, there are also many interesting progresses with bottom-up methods. One promising approach is the combination of chemistry and microfluidics technology, which creates clusters of particles in large numbers in solutions that stabilize the total SERS signal during measurements [81]. This method is based on microfluidic chips, so it can be easily combined with pretreatment functions, i.e., separation and enrichment, making it a powerful tool for real-world applications.

In recent years, there has been growing interest in exploring novel SERS-active substrates to enhance the Raman signals of target molecules. One work reports Mo2C as a highly sensitive semiconductor substrate [82], and another uses hat-shaped MoS2 films to separate two layers of metal nanoparticles and exhibits superior SERS capability [83]. These recent works collectively contribute to the understanding of 2D films as SERS-active substrates and showcase their potential as promising candidates for sensitive molecular detection and spectroscopic analyses.

In addition, new measurement techniques for SERS were also developed to meet the request of different application scenarios. One example is the surface-enhanced spatially offset Raman spectroscopy (SESORS) [84]. By introducing a spatial offset between the excitation and detection optical paths, it allows selective detection of the Raman signal from deep tissues [85,86]. Another important SERS measurement technique is the fiber-

integrated SERS substrate. In recent decades, different design and fabrication strategies were developed. The flexibility of the fiber system extended the detection to environments that cannot be reached by traditional substrates, such as tissues, cells, and harsh environments [87,88].

Today, SERS is not only used for the detection of trace amounts of chemicals but has also been applied in complex systems, for example, the detection and photothermal sterilization of bacteria [89] and intracellular detections using single-particle SERS. In situ real-time detection and tracing of various chemicals in cells are essential for understanding the basic processes of life. The current main method involves using gene editing technology to make specific proteins have luminescent properties and observing and analyzing them under fluorescence microscopy. While achieving great success, fluorescence methods also have limitations. They require labeling and also face difficulties in detecting small molecules. But SERS does not suffer from these issues. It enhances the signal of any molecule which is absorbed on nanoparticles, making SERS a suitable tool for the detection of small molecules, especially metabolism-related small molecules [90–94]. For more relevant developments in this field, one can read a related review article by Ren [37].

The above ability to detect chemical substances in complex systems shows the great potential of SERS in medical diagnosis [95,96]. For example, SERS has been proven to be a sensitive and effective method for detecting cancer [97–100]. Other applications include the detection of HIV and COVID-19 [95]. Researchers have demonstrated a reliable detection of COVID-19 based on soft SERS substrates [101].

SERS can also be used as a powerful tool for food safety and environmental detection. In the past two decades, there have been significant advances in these fields, which have been well summarized in recent review articles [102–105].

When talking about SERS, one also needs to mention tip-enhancement Raman spectroscopy (TERS) (Figure 5g), which is the combination of SERS and scanning probe microscopy. TERS utilizes a sharp metallic tip as a single "hot spot". By scanning the "hot spot" and collecting SERS signals point-by-point, one can map the chemical information of a sample at nanometer resolution with single-molecule sensitivity [106,107]. This provides researchers with a powerful tool for understanding the composition of various chemical compositions and chemical reactions at interfaces [71,108–110]. Despite its huge successes, today, the application of TERS is still limited, and it takes a lot of effort to obtain a high-quality TERS image. One of the main reasons is the reliability of the probes used. The fabrication of high-performance, chemically stable probes that are not easily damaged or contaminated is still a challenging issue in this field.

Another important issue with TERS is that it requires a complex and expensive optical system to excite and collect the Raman signal from the tip. This system needs to be well integrated with a scanning probe microscope, and the precision of aligning the optical beam with the tip-end needs to be subwavelength. To address this issue, one way is to integrate the metallic probe with waveguides, which can guide the excitation light to the tip apex and collect the signal from the metallic tip to far-field detectors. For example, Liu and his colleagues developed the nanowire-fiber integrated tip, which can be directly used with a commercial scanning tunneling microscope without any additional supporting optical system [111]. This greatly simplified the design of TERS systems.

3.2. Surface-Enhanced Absorption Spectroscopies

UV-Vis absorption spectroscopy and IR absorption spectroscopy are the two most widely used spectroscopic tools in analytical laboratories. In particular, IR spectroscopy, like Raman spectroscopy, is the fingerprint spectroscopy for chemical analysis, and the information of molecular functional groups can be accurately obtained through the analysis of characteristic absorption peaks, which has many applications in material science, surface science, and other fields.

Conventionally, surface-enhanced infrared absorption spectroscopy (SEIRA) is mainly performed with metal plasmon antennas using the local field enhancement effect [67,112,113].

However, in the infrared region, metals tend to be perfect conductors, and their performance is close to that of traditional antennas. The signal enhancement caused by the resonance of the materials discussed earlier is not significant as in the case of the visible or near-IR regime. To this end, similar to the development of substrates for SERS, new vertical antenna-based coupled designs were introduced, which greatly improved the performance of the enhanced spectrum [114].

Interestingly, it has been found that graphene provides excellent properties in the IR region that traditional metal structures do not have. For graphene, the concentration of its conductive electrons is relatively low compared with metals, and its plasmon frequency is therefore in the IR regime instead of the visible range. Moreover, graphene is atomically thin, and this causes strong field enhancement at the edges, which are extremely sharp. Thanks to the above properties, graphene substrates have received a lot of attention in the field of SEIRA [115,116]. However, compared with SERS, the sensitivity of SEIRA is relatively low and cannot reach the single-molecule level. In addition, optical components are expensive for the IR regime. This limits the application of SEIRA.

There are also reports on surface-enhanced UV-Vis absorption spectroscopy, but the number is much lower compared with SERIA and SERS. This is because of several different factors, mainly the limitation of materials, the high price of optical equipment, and the lack of structural information in the ultraviolet spectral region. Moreover, the intrinsic absorption section of organic molecules in the UV-Vis regime is relatively large, and in most cases, the sensitivity already meets the requirements.

3.3. Surface-Enhanced Fluorescence

Surface-enhanced fluorescence (SEF) also has a long history, similar to the case of SERS. However, because the signal intensity of commonly used fluorescent molecules is much stronger than that of Raman scattering and infrared absorption, single-molecule fluorescence detection and tracing at room temperature can be achieved without any enhancement, and surface-enhanced fluorescence has received far less attention in chemical analysis than SERS and SEIRA.

This situation changed considerably after near-IR (NIR) dyes became popular in bioimaging in bio-/chem-sensing. Compared with fluorescence techniques in the visible range, near-infrared dyes offer a larger penetration depth in tissue imaging and lower background thanks to their low autofluorescence background. These properties make NIR dyes very popular for in vivo bioimaging and enzyme-linked immunosorbent assays (ELISA). However, the absorption cross-section of NIR dyes is much smaller than that in the visible or UV spectral range, and the fluorescence yield is often less than 10%. These properties bring up the issue of low signal again in a way similar to Raman spectroscopy, and it is therefore important to find ways to enhance the fluorescence of NIR dyes.

To address this, Chou's group developed a vertically coupled antenna-based technology [74,117], which can enhance the average fluorescence by thousands of times, and at "hot spots", the fluorescence signal can be enhanced by up to six orders of magnitude [73,118]. Using this method, the detection limit of the Ebola virus was successfully pushed to sub-fM [119]. This technology is compatible with existing ELISA detection equipment, and using nanoimprinting technology, plasmon substrates themselves can be prepared in large quantities. It is believed that this high-performance SEF-based technique will play an increasingly important role in the field of high-sensitivity detection, especially in the early diagnosis of major diseases.

4. Index Sensing and Laser-Induced Ionization with Plasmonic Nanostructures

In this section, we review the applications of plasmonic nanostructures based on more complex effects, such as optical forces and photothermal effects.

4.1. Refractive Index Sensing

As aforementioned, the resonance frequency of a plasmon resonance mode can be shifted by the presence of external analytes due to the works of optical forces. This effect makes plasmonic nanostructures an important tool for index sensing in chemistry (Table 1). Researchers have invested great enthusiasm in developing different types of refractive index sensors, and different reading and processing methods were also developed. Today, thin-film-based SPR sensors (Figure 6a) have become the gold standard for many applications in bio-/chem-analysis with a sensitivity down to 10^{-7} RIU, and they have been well documented by review works by different groups. We therefore only focus on individual nanostructure-based sensors as well as array structures, which are less covered.

Table 1. Comparison between SPR, LSPR, and ELISA.

	SPR	LSPR	ELISA
Label-free	Yes	Yes	No
Sensitivity	10^{-6} nm/RIU	10^{-2} nm/RIU	10^{-18} M [119]
Single-molecule detection	No	Yes [120]	Yes
Detection mode	Absorption wavelength/angle, imaging	Scattering, extinction, imaging	Fluorescence, imaging
Spatial resolution	10 μm	1 μm	1 μm
Real-time detection	Yes	Yes	No
Multiplexing	Yes	Yes	Yes

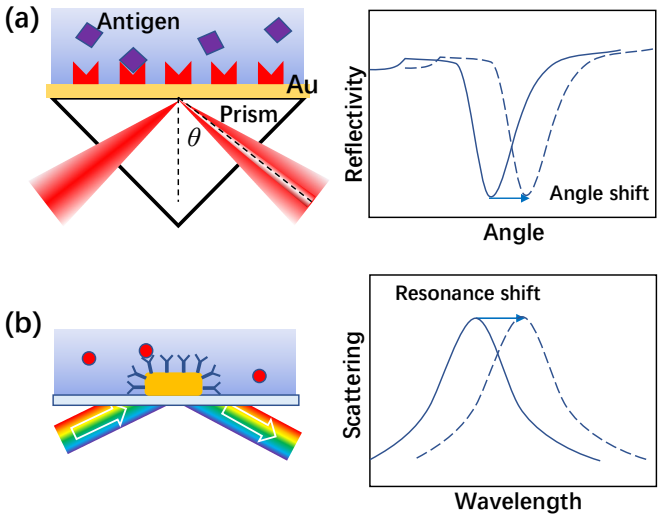

Figure 6. Principle of SPR sensor (**a**) and LSPR sensor (**b**).

Figure 6 shows the principle of this type of sensor. For a plasmonic nanoparticle, when a single molecule or viral particle is adsorbed on it, the resonance wavelength will undergo a step-like shift due to a change of the system's energy (Figure 6b), allowing us to probe a single particle or even single molecule in its local environment [17,121,122]. Array structures were also reported. They are mainly used for measuring the average concentration of solutions via continuous resonance shifts induced by global index changes [123].

Compared with conventional sensors, individual nanostructure-based LSRP sensors offer better sensitivity and spatial information. In recent decades, many interesting results have been reported using individual nanostructure-based LSPR sensors. For example, using separated plasmonic nanorods, researchers demonstrated the detection of single pro-

tein molecules [120]. When further combined with plasmon nano-antennas and traditional whispering-gallery-mode microcavities, the sensitivity can be further improved [124–126]. These above methods are based on the displacement detection of formants, which requires sophisticated spectroscopic equipment. Interestingly, it has been reported that by using nanopore design, optical detection of single molecules can be achieved by measuring the transmission intensity directly without requiring sophisticated spectroscopic equipment [127–129].

Due to their small size, plasmonic nanoparticles can even be used to detect local chemical information in living cells. This is because their scattering spectra can still be clearly recorded with dark-field imaging spectrographic instruments even after being injected into tissues [130,131]. Thanks to the high sensitivity and stability of plasmonic nanoparticles, they are expected to play an increasingly important role in in situ real-time analysis for life science in the future.

LSPR sensors can also be integrated with optical fibers [132,133]. In fact, fibers can be used for index sensing themselves using their own optical modes, such as the lossy-mode resonance (LMR)-based sensing technique [134–138]. The integration of LSPR can improve the sensitivity of the fiber-based sensors and further enable the combination of the SERS technique.

Thanks to their high sensitivity and ease of use, SPR and LSPR are now widely used in a variety of applications. Compared to ELISA, they can detect dynamic processes, which makes SPR technology particularly important in measuring molecular binding processes.

4.2. Photothermal Effects and Their Applications in Mass Spectrometry

As aforementioned, plasmonic nanostructures often exhibit strong photothermal effects. With their large light absorption cross-section and nanoscale volume, plasmonic nanostructures can be instantly heated to hundreds or even thousands of degrees when excited by laser pulses. This high temperature can be used to melt, desorb, and even break chemical bonds of the sample, making plasmonic nanostructures an interesting choice for building ion sources for MS measurements.

In MS, laser-induced desorption/ionization (LDI) is one of the most important ionization techniques for biomolecules [139,140]. It often uses small organic molecules as an assisting material to improve the efficiency of LDI and soften the ionization process of biomolecules. In the matrix-assisted LDI (MALDI) technique, the matrix molecules are ionized first, immediately after being hit by laser pulses, and then they transfer their charges to the target sample molecules. Because the energy is mainly absorbed by the matrix molecules, it does not destroy the structure of the organic analyte and can consequently avoid fragmentation issues. However, due to the presence of matrix molecules, there is always a high background noise level in the low mass regime. To address this issue, people developed surface-assisted laser desorption/ionization (SALDI) technology, which uses the photothermal effect of micro- and nanostructures to achieve the efficient, background-free desorption and ionization of organic molecules [141].

To date, many different types of nanostructures have been used for SALDI, but surprisingly, plasmonic nanostructures did often not show any advantages over nanostructures made of other materials until very recently [142,143]. This is because most of the plasmonic nanostructures are designed for surface-enhanced spectroscopies and are not optimized for the photothermal effect. Things only started to change in recent years. With the understanding of plasmon photothermal effects becoming deeper, high-performance plasmonic photothermal nanostructures were continuously reported. In particular, porous plasmonic nanostructures have emerged, which exhibit extremely high absorption efficiency, small heat capacity, and low thermal conductivity at the same time [18,19]. Using this structure, the authors successfully demonstrated the ionization of biomolecules. The results showed that its ionization efficiency is several times higher than the case of traditional MALDI substrates without background noise in the low mass charge region (Figure 7) [58].

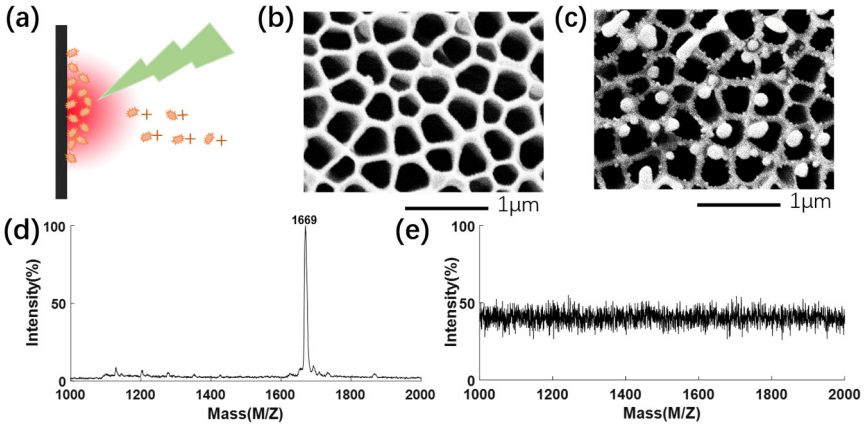

Figure 7. Plasmon-assisted laser desorption/ionization [58]. (**a**) Principle of laser desorption/ionization. (**b**,**c**) Porous plasmonic substrate before and after laser excitation. (**d**) Plasmonic substrate leads to a strong and clean signal. (**e**) No signal can be observed without the substrate.

It is worth noting that the strong photothermal effect can also lead to the complete dissociation of molecules and the formation of plasma. This allows plasmon structures to be applied to atomic spectroscopy (LIPS, laser-induced plasma spectroscopy).

5. Metasurface-Based Chemical Sensing and Analysis

In the previous section, all the applications are based on the properties of the individual nanostructures or uniform structure arrays. In this section, we will discuss the application of nonuniform nanostructure arrays (i.e., metasurfaces). They can map the hidden optical information into directly detectable intensity information, opening up many new possibilities for simplification and miniaturization of conventional analytical techniques.

5.1. Plasmonic Gradient as a Miniaturized Bio-Sensor

With the development of information technologies, particularly the Internet of Things (IoTs), people began to imagine that diagnostic equipment should be more personalized and decentralized, utilizing smart miniaturized point-of-care testing (POCT) equipment [144–146]. In recent years, the emergence of various new high-performance miniaturized chemical and biochemical sensors is making this dream a reality. Especially, plasmonic sensors (e.g., SPR and LSPR sensors) exhibit great potential for building such devices thanks to their small size and high signal strength. Meanwhile, the fast growth of consumer electronics, smartphones, and smartwatches started to integrate communication, computing, and advanced imaging functions together. It makes the integration of SPR/LSPR sensors and mobile phones a very promising direction [146,147].

The major function of SPR and LSPR sensors is to convert the refractive index information into absorption spectra or angular spectra that can be read by optical inspection equipment [148]. However, reading both absorption spectra and angular spectra requires additional equipment. To simplify the measurement, transmission or reflection signals at a single fixed wavelength are often used instead of the full spectra, but it is at the expense of measurement accuracy. To address the above issue, the authors propose an image-based ultrasensitive sensing method using gradient plasmon structures (plasmon metasurfaces), as shown in Figure 8 [149,150]. It is a 2D array of plasmonic nanorods whose resonance wavelength continuously varies from the center to the edge. When illuminated by a monochromic light source, the light will be absorbed at the position where the resonance matches the wavelength of the excitation light, and this will lead to a dark resonant ring. If the surrounding environment changes, the size of the ring will change too due to the resonant wavelength shift of the plasmonic nanorods. Such pattern changes can be accurately recorded and analyzed by mobile phones for ultrasensitive sensing purposes (as shown in Figure 8b,c). The results show that its sensitivity is comparable to large research-level instruments.

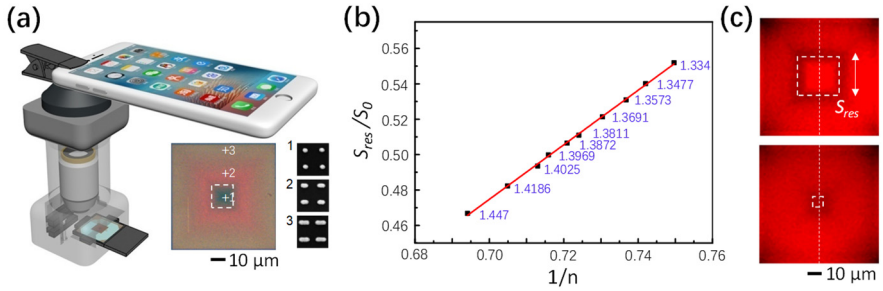

Figure 8. Smartphone-based plasmonic sensors. (**a**) A patterned plasmonic gradient sensor and its reader are capable of quantitatively measuring the environmental refractive index. (**b**) The size of the resonance ring, S_{res}, changes when the refractive index of the surrounding medium, n, changes. (**c**) S_{res} is linearly related to 1/n [150].

In addition to refractive index sensors based on local plasmon resonance, people have also tried to combine handheld spectrometers and surface-enhanced fluorescence sensors. In theory, this should lead to higher sensitivity compared to the LSPR-based sensors, but it also requires expensive light sources, filters, and more complex optics.

5.2. Snapshot CD Spectroscopy with a Metasurface

With the emergence of metasurfaces, we are gaining unprecedented light manipulation capability, leading to many new opportunities for the miniaturization of analysis instruments, including optical imaging, polarization measurements, and spectral analysis. Today, there have been a few reviews on optical imaging applications [30,59]; therefore, and we limit our discussion on polarization analysis, more specifically, CD spectroscopy, which is important for biochemical analysis.

CD spectroscopy measures the difference between optical interactions with left- and right-handed circular polarized light. It is the most widely used characterization method for measuring the chirality of molecules, having many important applications in chemistry, life science, and medicine. Because the CD signals are several orders of magnitude weaker than traditional spectroscopic signals, it requires complex optical modulation–demodulation equipment to retrieve them [151]. This makes CD spectroscopy a complex and expensive analytical technique.

Interestingly, with the help of polarization gratings, the measurement for CD spectra can be greatly simplified. The polarization grating is essentially a metasurface, which diffracts left-handed and right-handed circular polarized components of light into different directions with equal efficiencies [152]. The CD measurement can therefore be performed by simply collecting signals with different polarizations at the same wavelength and calculating their differences. In addition, polarization gratings can be coupled to microscopic imaging systems, making it possible to collect signals from a single nanostructure, as shown in Figure 9. Using this method, the authors and collaborators developed the snapshot CD spectroscopy technique and demonstrated the CD spectroscopy of single DNA-assembled 3D nanostructures [35].

It should be noted here that the polarization grating used here is made of liquid crystals instead of metallic nanostructures because liquid crystals are adjustable, transparent, and convenient to process. It is also possible to fabricate polarization gratings with dielectric or metallic nanostructures, but the nanofabrication is much more expensive than the case of liquid crystals.

Finally, it is worth noting that with the emergence of the metasurface technique, the boundaries between imaging, spectrometry, and polarimetry in conventional optical design are becoming blurred. One can map the spectral and polarization information from any spatial point in a sample onto intensity distributions on any given plane, which then can be recorded with imaging devices. This unique capability is particularly important today because high-quality imaging devices with a large format have become available in our daily life. For instance, the pixel number of the CMOS sensor in a smartphone has reached

100 million. One can therefore expect that high-performance and ultracompact spectropolarimetric imaging devices will be integrated into consumer electronic products in the near future. This will dramatically change the landscape of chemical sensing and analysis.

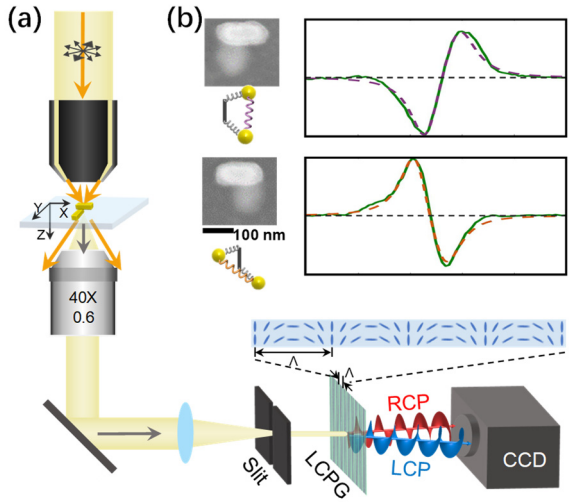

Figure 9. Snapshot CD spectroscopy of single nanostructure using a polarization grating [35]. (**a**) Schematic drawing of the CD spectrometer. (**b**) Scattering CD spectra of right-hand and left-hand enantiomer, respectively. The insets are the SEM images of the nanostructures.

6. Applications in Life Science and Theranostics

As discussed above, plasmons can be used as nanoscale optical sensors, energy converters, and spectral signal amplifiers. These properties offer great potential applications for plasmons in life sciences and diagnostics.

Intracellular plasmonics is a cutting-edge field focusing on the use of plasmonic nanostructures within living cells. By introducing these nanostructures, researchers can enhance imaging contrast, enable targeted therapies, and probe cellular processes at the nanoscale [153–156]. For example, one work reports that by using multifunctional gold nanoparticles, these intracellular sensors can monitor actin rearrangement in live fibroblasts [157]. Another work shows an electrochemical impedance microscope based on surface plasmon resonance that resolves local impedance with submicrometer spatial resolution and monitors the dynamics of cellular processes with millisecond time resolution [158]. Intracellular plasmonics offers novel insights into cell biology and holds great potential for revolutionizing cell-based research and personalized medicine.

In recent years, plasmonic nanoparticles have emerged as key players in advancing theranostics. These nanoparticles enhance imaging contrast in techniques like SERS and photoacoustic imaging while serving as efficient carriers for site-specific drug release [159,160]. Additionally, plasmons enable novel treatments like photothermal therapy, where localized heating selectively destroys cancer cells [20,161,162]. Nowadays, many novel plasmonic nanoparticles have been applied to theranostics. For example, plasmonic nanobubbles lead to rapid heating and vaporization of the surrounding medium, which has been explored for targeted drug delivery and tumor ablation [163]. Another example is gap-enhanced Raman tags (GERTs), which are a class of nanoscale structures that significantly amplify the Raman scattering signal of molecules attached to or within their nanogap regions. These GERTs have been applied as the second near-infrared window (NIR-II) SERS tags and achieved successes from biodetection to theranostics owing to their simultaneous extra-high SERS response, ultra-photostability, and multiplexing capability [164,165]. The development of plasmons in theranostics holds great promise for personalized and effective healthcare.

7. Summary and Outlook

From the above review, it can be seen that optical nanostructures, especially plasmon nanostructures, can significantly enhance the optical effects at the nanoscale, which are otherwise extremely weak. These nanostructures can therefore function as a bridge that connects the nanoscale chemical information in its near field to the far-field propagating waves, allowing researchers to collect and analyze the spectral information from trace amounts of samples or even a single molecule. In the last decade, the field of nano-optics has become mature. With the development of computational electromagnetic technology and nanofabrication technology, the design and fabrication of plasmonic sensors have become standard processes. The focus of research has begun to shift from conventional surface-enhanced spectroscopies to applications that involve complex multi-physical effects, such as LSPR-based sensing and SALDI. The former is associated with the near-field optical trapping phenomenon, and the latter relies on the nanoscale temporal photothermal processes of plasmonics.

Another important trend for nanostructure-based chemical analysis is integration and miniaturization. Today, sensing techniques for physical signals have matured, but there is still a lack of biochemical sensors which are small, integrated, and highly selective. At the same time, information techniques, especially IoT techniques, are growing at a breathtaking speed, and the demand for real-time and reliable monitoring methods of biochemical information for the environment, public safety, and health is becoming increasingly urgent. Optical nanostructures, such as plasmonics and metasurfaces, provide an attractive solution for high-performance, miniaturized, and low-cost sensors. We believe that driven by the market, the development of reliable, highly selectable, and integrable nanostructure-based biochemical sensors will be an important trend in the next decade.

Finally, it is worth mentioning that optical measurement methods have made significant progress in the last decade. Nonlinear optics and quantum optics technologies have begun to make their way from basic research to various application fields, including sensing [166,167]. It has been experimentally demonstrated that nonlinear and quantum effects can improve the performance of optical nanostructure-based sensors, such as the signal-to-noise ratio and accuracy [168–171]. We believe that this will bring many new opportunities in the future.

Author Contributions: Writing—original draft preparation, C.D. and W.Z.; surface-enhanced spectroscopy Y.W.; theoretical part, X.Z.; LSPR sensor, J.B. All authors have read and agreed to the published version of the manuscript.

Funding: This research was funded by National Key Technologies R&D Program of China (No. 2021YFA1400803).

Informed Consent Statement: Not applicable here.

Data Availability Statement: Not applicable.

Conflicts of Interest: The authors declare no conflict of interest.

References

1. McHale, J.L. *Molecular Spectroscopy*, 2nd ed.; CRC Press: Boca Raton, FL, USA, 2017.
2. Koleżyński, A.; Król, M. *Molecular Spectroscopy—Experimental and Theroy*; Springer: Berlin/Heidelberg, Germany, 2019; Volume 26.
3. Lal, S.; Link, S.; Halas, N.J. Nano-optics from sensing to waveguiding. *Nat. Photonics* **2007**, *1*, 641–648. [CrossRef]
4. Willets, K.A.; Van Duyne, R.P. Localized Surface Plasmon Resonance Spectroscopy and Sensing. *Annu. Rev. Phys. Chem.* **2007**, *58*, 267–297. [CrossRef]
5. Homola, J. Surface plasmon resonance sensors for detection of chemical and biological species. *Chem. Rev.* **2008**, *108*, 462–493. [CrossRef] [PubMed]
6. Pohl, D.W.; Kawata, S.; Inouye, Y.; Fischer, U.C.; Dereux, A.; Weeber, J.-C.; Hayashi, S.; Okamoto, T.; Novotny, L.; Sugiura, T.; et al. *Near-Field Optics and Surface Plasmon Polaritons*; Kawata, S., Ed.; Springer: Berlin/Heidelberg, Germany, 2001.
7. Maier, S.A. *Plasmonics: Fundamentals and Applications*; Springer Science & Business Media: Berlin/Heidelberg, Germany, 2007.
8. Novotny, L.; Hecht, B. *Principles of Nano-Optics*; Cambridge University Press: Cambridge, UK, 2012.
9. Bohren, C.F.; Huffman, D.R. *Absorption and Scattering of Light by Small Particles*; John Wiley & Sons, Inc.: Hoboken, NJ, USA, 1983.

10. Raether, H. *Surface Plasmons on Smooth and Rough Surfaces and on Gratings*; Springer: Berlin/Heidelberg, Germany, 1989.
11. Kreibig, U.; Vollmer, M. *Optical Properties of Metal Clusters*; Springer: Berlin/Heidelberg, Germany, 1995; Volume 25.
12. Kneipp, K.; Wang, Y.; Kneipp, H.; Perelman, L.T.; Itzkan, I.; Dasari, R.R.; Feld, M.S. Single Molecule Detection Using Surface-Enhanced Raman Scattering (SERS). *Phys. Rev. Lett.* **1997**, *78*, 1667. [CrossRef]
13. Nie, S.; Emory, S.R. Probing Single Molecules and Single Nanoparticles by Surface-Enhanced Raman Scattering. *Science* **1997**, *275*, 1102–1106. [CrossRef]
14. Englebienne, P. Use of colloidal gold surface plasmon resonance peak shift to infer affinity constants from the interactions between protein antigens and antibodies specific for single or multiple epitopes. *Analyst* **1998**, *123*, 1599–1603. [CrossRef]
15. Mulvaney, P. Surface Plasmon Spectroscopy of Nanosized Metal Particles. *Langmuir* **1996**, *12*, 788–800. [CrossRef]
16. Ament, I.; Prasad, J.; Henkel, A.; Schmachtel, S.; Soennichsen, C. Single Unlabeled Protein Detection on Individual Plasmonic Nanoparticles. *Nano Lett.* **2012**, *12*, 1092–1095. [CrossRef]
17. Pang, Y.; Gordon, R. Optical Trapping of a Single Protein. *Nano Lett.* **2012**, *12*, 402–406. [CrossRef]
18. Hogan, N.J.; Urban, A.S.; Ayala-Orozco, C.; Pimpinelli, A.; Nordlander, P.; Halas, N.J. Nanoparticles Heat through Light Localization. *Nano Lett.* **2014**, *14*, 4640–4645. [CrossRef]
19. Zhou, L.; Tan, Y.L.; Wang, J.Y.; Xu, W.C.; Yuan, Y.; Cai, W.S.; Zhu, S.N.; Zhu, J. 3D self-assembly of aluminium nanoparticles for plasmon-enhanced solar desalination. *Nat. Photonics* **2016**, *10*, 393. [CrossRef]
20. Huang, X.; Jain, P.K.; El-Sayed, I.H.; El-Sayed, M.A. Plasmonic photothermal therapy (PPTT) using gold nanoparticles. *Lasers Med. Sci.* **2008**, *23*, 217–228. [CrossRef]
21. Krioukov, E.; Klunder, D.J.W.; Driessen, A.; Greve, J.; Otto, C. Sensor based on an integrated optical microcavity. *Opt. Lett.* **2002**, *27*, 512–514. [CrossRef]
22. Vollmer, F.; Braun, D.; Libchaber, A.; Khoshsima, M.; Teraoka, I.; Arnold, S. Protein detection by optical shift of a resonant microcavity. *Appl. Phys. Lett.* **2002**, *80*, 4057–4059. [CrossRef]
23. Armani, A.M.; Kulkarni, R.P.; Fraser, S.E.; Flagan, R.C.; Vahala, K.J. Label-free, single-molecule detection with optical microcavities. *Science* **2007**, *317*, 783–787. [CrossRef]
24. Sun, Y.Z.; Fan, X.D. Optical ring resonators for biochemical and chemical sensing. *Anal. Bioanal. Chem.* **2011**, *399*, 205–211. [CrossRef] [PubMed]
25. Rho, D.; Breaux, C.; Kim, S. Label-Free Optical Resonator-Based Biosensors. *Sensors* **2020**, *20*, 5901. [CrossRef] [PubMed]
26. Yu, N.F.; Genevet, P.; Kats, M.A.; Aieta, F.; Tetienne, J.P.; Capasso, F.; Gaburro, Z. Light Propagation with Phase Discontinuities: Generalized Laws of Reflection and Refraction. *Science* **2011**, *334*, 333–337. [CrossRef] [PubMed]
27. Yu, N.F.; Capasso, F. Flat optics with designer metasurfaces. *Nat. Mater.* **2014**, *13*, 139–150. [CrossRef] [PubMed]
28. Khorasaninejad, M.; Chen, W.T.; Devlin, R.C.; Oh, J.; Zhu, A.Y.; Capasso, F. Metalenses at visible wavelengths: Diffraction-limited focusing and subwavelength resolution imaging. *Science* **2016**, *352*, 1190–1194. [CrossRef]
29. Khorasaninejad, M.; Chen, W.T.; Oh, J.; Capasso, F. Super-Dispersive Off-Axis Meta-Lenses for Compact High Resolution Spectroscopy. *Nano Lett.* **2016**, *16*, 3732–3737. [CrossRef]
30. Faraji-Dana, M.; Arbabi, E.; Kwon, H.; Kamali, S.M.; Arbabi, A.; Bartholomew, J.G.; Faraon, A. Hyperspectral Imager with Folded Metasurface Optics. *ACS Photonics* **2019**, *6*, 2161–2167. [CrossRef]
31. Rubin, N.A.; D'Aversa, G.; Chevalier, P.; Shi, Z.J.; Chen, W.T.; Capasso, F. Matrix Fourier optics enables a compact full-Stokes polarization camera. *Science* **2019**, *365*, eaax1839. [CrossRef] [PubMed]
32. Wang, R.X.; Ansari, M.A.; Ahmed, H.; Li, Y.; Cai, W.F.; Liu, Y.J.; Li, S.T.; Liu, J.L.; Li, L.; Chen, X.Z. Compact multi-foci metalens spectrometer. *Light Sci. Appl.* **2023**, *12*, 103. [CrossRef]
33. Solomon, M.L.; Abendroth, J.M.; Poulikakos, L.V.; Hu, J.; Dionne, J.A. Fluorescence-Detected Circular Dichroism of a Chiral Molecular Monolayer with Dielectric Metasurfaces. *J. Am. Chem. Soc.* **2020**, *142*, 18304–18309. [CrossRef]
34. Lin, P.; Chen, W.T.; Yousef, K.M.A.; Marchioni, J.; Zhu, A.; Capasso, F.; Cheng, J.X. Coherent Raman scattering imaging with a near-infrared achromatic metalens. *APL Photonics* **2021**, *6*, 096107. [CrossRef] [PubMed]
35. Zhou, S.; Bian, J.; Chen, P.; Xie, M.; Chao, J.; Hu, W.; Lu, Y.Q.; Zhang, W.H. Polarization-dispersive imaging spectrometer for scattering circular dichroism spectroscopy of single chiral nanostructures. *Light Sci. Appl.* **2022**, *11*, 64. [CrossRef] [PubMed]
36. Graham, D.; Moskovits, M.; Tian, Z.-Q. SERS—Facts, figures and the future. *Chem. Soc. Rev.* **2017**, *46*, 3864–3865. [CrossRef]
37. Zong, C.; Xu, M.; Xu, L.-J.; Wei, T.; Ma, X.; Zheng, X.-S.; Hu, R.; Ren, B. Surface-Enhanced Raman Spectroscopy for Bioanalysis: Reliability and Challenges. *Chem. Rev.* **2018**, *118*, 4946–4980. [CrossRef]
38. Mayer, K.M.; Hafner, J.H. Localized Surface Plasmon Resonance Sensors. *Chem. Rev.* **2011**, *111*, 3828–3857. [CrossRef] [PubMed]
39. Gu, Y.; Chen, L.; Zhang, H.; Gong, Q. Resonance capacity of surface plasmon on subwavelength metallic structures. *EPL* **2008**, *83*, 27004. [CrossRef]
40. Wang, F.; Shen, Y.R. General Properties of Local Plasmons in Metal Nanostructures. *Phys. Rev. Lett.* **2006**, *97*, 206806. [CrossRef] [PubMed]
41. Zhang, W.; Gallinet, B.; Martin, O.J.F. Symmetry and selection rules for localized surface plasmon resonances in nanostructures. *Phys. Rev. B* **2010**, *81*, 233407. [CrossRef]
42. Zhang, W. A general theory for plasmonic nanosensor. In Proceedings of the 2015 International Conference on Optical Instruments and Technology: Optical Sensors and Applications, Beijing, China, 8–10 May 2015; p. 2193396.

43. Muhlschlegel, P.; Eisler, H.J.; Martin, O.J.F.; Hecht, B.; Pohl, D.W. Resonant optical antennas. *Science* **2005**, *308*, 1607–1609. [CrossRef]
44. Novotny, L. Effective wavelength scaling for optical antennas. *Phys. Rev. Lett.* **2007**, *98*, 266802. [CrossRef] [PubMed]
45. Bharadwaj, P.; Deutsch, B.; Novotny, L. Optical Antennas. *Adv. Opt. Photonics* **2009**, *1*, 438–483. [CrossRef]
46. Milligan, T.A. *Modern Antenna Design*, 2nd ed.; John Wiley & Sons, Inc.: Hoboken, NJ, USA, 2005.
47. Le Ru, E.; Etchegoin, P. *Principles of Surface-Enhanced Raman Spectroscopy: And Related Plasmonic Effects*; Elsevier: London, UK, 2009.
48. Buchler, B.C.; Kalkbrenner, T.; Hettich, C.; Sandoghdar, V. Measuring the quantum efficiency of the optical emission of single radiating dipoles using a scanning mirror. *Phys. Rev. Lett.* **2005**, *95*, 063003. [CrossRef] [PubMed]
49. Kuehn, S.; Hakanson, U.; Rogobete, L.; Sandoghdar, V. Enhancement of single-molecule fluorescence using a gold nanoparticle as an optical nanoantenna. *Phys. Rev. Lett.* **2006**, *97*, 017402. [CrossRef]
50. Martin, O.J.F.; Girard, C.; Dereux, A. Generalized Field Propagator for Electromagnetic Scattering and Light Confinement. *Phys. Rev. Lett.* **1995**, *74*, 526–529. [CrossRef]
51. Chance, R.R.; Prock, A.; Silbey, R. Molecular Fluorescence and Energy Transfer Near Interfaces. *Adv. Chem. Phys.* **1978**, *37*, 1–65.
52. Kang, K.A.; Wang, J.; Jasinski, J.B.; Achilefu, S. Fluorescence Manipulation by Gold Nanoparticles: From Complete Quenching to Extensive Enhancement. *J. Nanobiotechnol.* **2011**, *9*, 16. [CrossRef]
53. Brouwer, A.M. Standards for photoluminescence quantum yield measurements in solution (IUPAC Technical Report). *Pure Appl. Chem.* **2011**, *83*, 2213–2228. [CrossRef]
54. Kotnala, A.; Gordon, R. Double nanohole optical tweezers visualize protein p53 suppressing unzipping of single DNA-hairpins. *Biomed. Opt. Express* **2014**, *5*, 1886–1894. [CrossRef]
55. Zhang, W.; Martin, O.J.F. Optical trapping and sensing with plasmonic dipole antennas. In *Plasmonics: Metallic Nanostructures and Their Optical Properties VIII*, Stockman, M.I., Ed.; Proceedings of SPIE; SPIE: Bellingham, WA, USA, 2010; Volume 7757, pp. 85–91.
56. Kotnala, A.; Gordon, R. Quantification of High-Efficiency Trapping of Nanoparticles in a Double Nanohole Optical Tweezer. *Nano Lett.* **2014**, *14*, 853–856. [CrossRef] [PubMed]
57. Zhang, W.H.; Martin, O.J.F. A Universal Law for Plasmon Resonance Shift in Biosensing. *ACS Photonics* **2015**, *2*, 144–150. [CrossRef]
58. Zhu, J.J.; Meng, X.; Zhang, C.; Bian, J.; Lu, Z.D.; Liu, Y.; Zhang, W.H. Tailoring a nanostructured plasmonic absorber for high efficiency surface-assisted laser desorption/ionization. *Phys. Chem. Chem. Phys.* **2018**, *20*, 3424–3429. [CrossRef]
59. Kamali, S.M.; Arbabi, E.; Arbabi, A.; Faraon, A. A review of dielectric optical metasurfaces for wavefront control. *Nanophotonics* **2018**, *7*, 1041–1068. [CrossRef]
60. Xie, X.; Liu, K.P.; Pu, M.B.; Ma, X.L.; Li, X.; Guo, Y.H.; Zhang, F.; Luo, X.G. All-metallic geometric metasurfaces for broadband and high-efficiency wavefront manipulation. *Nanophotonics* **2020**, *9*, 3209–3215. [CrossRef]
61. Jisha, C.P.; Nolte, S.; Alberucci, A. Geometric Phase in Optics: From Wavefront Manipulation to Waveguiding. *Laser Photonics Rev.* **2021**, *15*, 2100003. [CrossRef]
62. Fleischmann, M.; Hendral, P.J.; McQuillan, A.J. Raman spectra of pyridine adsorbed at a silver electrode. *Chem. Phys. Lett.* **1974**, *26*, 163–166. [CrossRef]
63. Jeanmaire, D.L.; Van Duyne, R.P. Surface Raman spectroelectrochemistry: Part I. Heterocyclic, aromatic, and aliphatic amines adsorbed on the anodized silver electrode. *J. Electroanal. Chem.* **1977**, *84*, 1–20. [CrossRef]
64. Moskovits, M. Surface roughness and the enhanced intensity of Raman scattering by molecules adsorbed on metals. *J. Chem. Phys.* **1978**, *69*, 4159–4161. [CrossRef]
65. Panneerselvam, R.; Liu, G.-K.; Wang, Y.-H.; Liu, J.-Y.; Ding, S.-Y.; Li, J.-F.; Wu, D.-Y.; Tian, Z.-Q. Surface-enhanced Raman spectroscopy: Bottlenecks and future directions. *Chem. Commun.* **2017**, *54*, 10–25. [CrossRef]
66. Xu, H.X.; Aizpurua, J.; Kall, M.; Apell, P. Electromagnetic contributions to single-molecule sensitivity in surface-enhanced Raman scattering. *Phys. Rev. E* **2000**, *62*, 4318–4324. [CrossRef]
67. Neubrech, F.; Pucci, A.; Cornelius, T.W.; Karim, S.; Garcia-Etxarri, A.; Aizpurua, J. Resonant Plasmonic and Vibrational Coupling in a Tailored Nanoantenna for Infrared Detection. *Phys. Rev. Lett.* **2008**, *101*, 157403. [CrossRef]
68. Novotny, L.; van Hulst, N. Antennas for light. *Nat. Photonics* **2011**, *5*, 83–90. [CrossRef]
69. Seok, T.J.; Jamshidi, A.; Kim, M.; Dhuey, S.; Lakhani, A.; Choo, H.; Schuck, P.J.; Cabrini, S.; Schwartzberg, A.M.; Bokor, J.; et al. Radiation engineering of optical antennas for maximum field enhancement. *Nano Lett.* **2011**, *11*, 2606–2610. [CrossRef] [PubMed]
70. Zhang, W.; Cui, X.; Yeo, B.-S.; Schmid, T.; Hafner, C.; Zenobi, R. Nanoscale roughness on metal surfaces can increase tip-enhanced Raman scattering by an order of magnitude. *Nano Lett.* **2007**, *7*, 1401–1405. [CrossRef]
71. Zhang, W.; Schmid, T.; Yeo, B.-S.; Zenobi, R. Near-field heating, annealing, and signal loss in tip-enhanced Raman spectroscopy. *J. Phys. Chem. C* **2008**, *112*, 2104–2108. [CrossRef]
72. Zhang, W. *Tip-Enhanced Raman Spectroscopy: Theory, Practice and Applications*; ETH Zurich: Zurich, Switzerland, 2008.
73. Zhang, W.; Ding, F.; Li, W.-D.; Wang, Y.; Hu, J.; Chou, S.Y. Giant and uniform fluorescence enhancement over large areas using plasmonic nanodots in 3D resonant cavity nanoantenna by nanoimprinting. *Nanotechnology* **2012**, *23*, 225301. [CrossRef] [PubMed]
74. Li, W.-D.; Ding, F.; Hu, J.; Chou, S.Y. Three-dimensional cavity nanoantenna coupled plasmonic nanodots for ultrahigh and uniform surface-enhanced Raman scattering over large area. *Opt. Express* **2011**, *19*, 3925–3936. [CrossRef]
75. Zhang, W.; Ding, F.; Chou, S.Y. Large Enhancement of Upconversion Luminescence of NaYF4:Yb3+/Er3+ Nanocrystal by 3D Plasmonic Nano-Antennas. *Adv. Mater.* **2012**, *24*, OP236–OP241. [CrossRef] [PubMed]

76. Moreau, A.; Ciraci, C.; Mock, J.J.; Hill, R.T.; Wang, Q.; Wiley, B.J.; Chilkoti, A.; Smith, D.R. Controlled-reflectance surfaces with film-coupled colloidal nanoantennas. *Nature* **2012**, *492*, 86–89. [CrossRef] [PubMed]
77. Benz, F.; Schmidt, M.K.; Dreismann, A.; Chikkaraddy, R.; Zhang, Y.; Demetriadou, A.; Carnegie, C.; Ohadi, H.; de Nijs, B.; Esteban, R.; et al. Single-molecule optomechanics in "picocavities". *Science* **2016**, *354*, 726–729. [CrossRef]
78. Chen, H.-Y.; Lin, M.-H.; Wang, C.-Y.; Chang, Y.-M.; Gwo, S. Large-Scale Hot Spot Engineering for Quantitative SERS at the Single-Molecule Scale. *J. Am. Chem. Soc.* **2015**, *137*, 13698–13705. [CrossRef]
79. Caridad, J.M.; Winters, S.; McCloskey, D.; Duesberg, G.S.; Donegan, J.F.; Krstić, V. Hot-Volumes as Uniform and Reproducible SERS-Detection Enhancers in Weakly-Coupled Metallic Nanohelices. *Sci. Rep.* **2017**, *7*, 45548. [CrossRef] [PubMed]
80. Li, J.F.; Huang, Y.F.; Ding, Y.; Yang, Z.L.; Li, S.B.; Zhou, X.S.; Fan, F.R.; Zhang, W.; Zhou, Z.Y.; Wu, D.Y.; et al. Shell-isolated nanoparticle-enhanced Raman spectroscopy. *Nature* **2010**, *464*, 392–395. [CrossRef]
81. Lu, H.; Zhu, L.; Zhang, C.; Chen, K.; Cui, Y. Mixing Assisted "Hot Spots" Occupying SERS Strategy for Highly Sensitive In Situ Study. *Anal. Chem.* **2018**, *90*, 4535–4543. [CrossRef]
82. Ji, C.; Lu, J.; Shan, B.; Li, F.; Zhao, X.; Yu, J.; Xu, S.; Man, B.; Zhang, C.; Li, Z. The Origin of Mo2C Films for Surface-Enhanced Raman Scattering Analysis: Electromagnetic or Chemical Enhancement? *J. Phys. Chem. Lett.* **2022**, *13*, 8864–8871. [CrossRef]
83. Zhang, C.; Li, Z.; Qiu, S.; Lu, W.; Shao, M.; Ji, C.; Wang, G.; Zhao, X.; Yu, J.; Li, Z. Highly ordered arrays of hat-shaped hierarchical nanostructures with different curvatures for sensitive SERS and plasmon-driven catalysis. *Nanophotonics* **2022**, *11*, 33–44. [CrossRef]
84. Stone, N.; Kerssens, M.; Lloyd, G.R.; Faulds, K.; Graham, D.; Matousek, P. Surface enhanced spatially offset Raman spectroscopic (SESORS) imaging—The next dimension. *Chem. Sci.* **2011**, *2*, 776–780. [CrossRef]
85. Moody, A.S.; Payne, T.D.; Barth, B.A.; Sharma, B. Surface-enhanced spatially-offset Raman spectroscopy (SESORS) for detection of neurochemicals through the skull at physiologically relevant concentrations. *Analyst* **2020**, *145*, 1885–1893. [CrossRef]
86. Asiala, S.M.; Shand, N.C.; Faulds, K.; Graham, D. Surface-Enhanced, Spatially Offset Raman Spectroscopy (SESORS) in Tissue Analogues. *ACS Appl. Mater. Interfaces* **2017**, *9*, 25488–25494. [CrossRef] [PubMed]
87. Managò, S.; Quero, G.; Zito, G.; Tullii, G.; Galeotti, F.; Pisco, M.; De Luca, A.C.; Cusano, A. Tailoring lab-on-fiber SERS optrodes towards biological targets of different sizes. *Sens. Actuators B* **2021**, *339*, 129321. [CrossRef]
88. Sansone, L.; Campopiano, S.; Pannico, M.; Giordano, M.; Musto, P.; Iadicicco, A. Photonic bandgap influence on the SERS effect in metal-dielectric colloidal crystals optical fiber probe. *Sens. Actuators B* **2021**, *345*, 130149. [CrossRef]
89. Jiang, L.; Yu, Z.; Zhao, W.; Yang, Z.; Peng, Y.; Zhou, Y.; Lin, X.; Jin, S. Self-Assembled MXene-Au Multifunctional Nanomaterials with Various Shapes for Label-free SERS Detection of Pathogenic Bacteria and Photothermal Sterilization. *Anal. Chem.* **2023**, *95*, 1721–1730. [CrossRef]
90. Stuart, D.A.; Yuen, J.M.; Lyandres, N.S.O.; Yonzon, C.R.; Glucksberg, M.R.; Walsh, J.T.; Van Duyne, R.P. In vivo glucose measurement by surface-enhanced Raman spectroscopy. *Anal. Chem.* **2006**, *78*, 7211–7215. [CrossRef]
91. Hsu, P.-H.; Chiang, H.K. Surface-enhanced Raman spectroscopy for quantitative measurement of lactic acid at physiological concentration in human serum. *J. Raman Spectrosc.* **2010**, *41*, 1610–1614. [CrossRef]
92. Ma, K.; Yuen, J.M.; Shah, N.C.; Walsh, J.T., Jr.; Glucksberg, M.R.; Van Duyne, R.P. In Vivo, Transcutaneous Glucose Sensing Using Surface-Enhanced Spatially Offset Raman Spectroscopy: Multiple Rats, Improved Hypoglycemic Accuracy, Low Incident Power, and Continuous Monitoring for Greater than 17 Days. *Anal. Chem.* **2011**, *83*, 9146–9152. [CrossRef]
93. Hu, P.; Zheng, X.-S.; Zong, C.; Li, M.-H.; Zhang, L.-Y.; Li, W.; Ren, B. Drop-coating deposition and surface-enhanced Raman spectroscopies (DCDRS and SERS) provide complementary information of whole human tears. *J. Raman Spectrosc.* **2014**, *45*, 565–573. [CrossRef]
94. Shen, W.; Lin, X.; Jiang, C.; Li, C.; Lin, H.; Huang, J.; Wang, S.; Liu, G.; Yan, X.; Zhong, Q.; et al. Reliable Quantitative SERS Analysis Facilitated by Core-Shell Nanoparticles with Embedded Internal Standards. *Angew. Chem. Int. Ed.* **2015**, *54*, 7308–7312. [CrossRef] [PubMed]
95. Yadav, S.; Senapati, S.; Desai, D.; Gahlaut, S.; Kulkarni, S.; Singh, J.P. Portable and sensitive Ag nanorods based SERS platform for rapid HIV-1 detection and tropism determination. *Colloids Surf. B Biointerfaces* **2021**, *198*, 111477. [CrossRef] [PubMed]
96. Beeram, R.; Vepa, K.R.; Soma, V.R. Recent Trends in SERS-Based Plasmonic Sensors for Disease Diagnostics, Biomolecules Detection, and Machine Learning Techniques. *Biosensors* **2023**, *13*, 328. [CrossRef] [PubMed]
97. Samanta, A.; Maiti, K.K.; Soh, K.S.; Liao, X.J.; Vendrell, M.; Dinish, U.S.; Yun, S.W.; Bhuvaneswari, R.; Kim, H.; Rautela, S.; et al. Ultrasensitive Near-Infrared Raman Reporters for SERS-Based In Vivo Cancer Detection. *Angew. Chem. Int. Ed.* **2011**, *50*, 6089–6092. [CrossRef] [PubMed]
98. Haldavnekar, R.; Venkatakrishnan, K.; Tan, B. Non plasmonic semiconductor quantum SERS probe as a pathway for in vitro cancer detection. *Nat. Commun.* **2018**, *9*, 3065. [CrossRef] [PubMed]
99. Guerrini, L.; Alvarez-Puebla, R.A. Surface-Enhanced Raman Spectroscopy in Cancer Diagnosis, Prognosis and Monitoring. *Cancers* **2019**, *11*, 748. [CrossRef]
100. Pollap, A.; Swit, P. Recent Advances in Sandwich SERS Immunosensors for Cancer Detection. *Int. J. Mol. Sci.* **2022**, *23*, 4740. [CrossRef]
101. Mousavi, S.M.; Hashemi, S.A.; Rahmanian, V.; Kalashgrani, M.Y.; Gholami, A.; Omidifar, N.; Chiang, W.H. Highly Sensitive Flexible SERS-Based Sensing Platform for Detection of COVID-19. *Biosensors* **2022**, *12*, 466. [CrossRef]

102. Lin, Z.S.; He, L.L. Recent advance in SERS techniques for food safety and quality analysis: A brief review. *Curr. Opin. Food Sci.* **2019**, *28*, 82–87. [CrossRef]
103. Zhou, H.L.; Li, X.D.; Wang, L.H.; Liang, Y.F.; Jialading, A.; Wang, Z.S.; Zhang, J.G. Application of SERS quantitative analysis method in food safety detection. *Rev. Anal. Chem* **2021**, *40*, 173–186. [CrossRef]
104. Kumar, S.; Goel, P.; Singh, J.P. Flexible and robust SERS active substrates for conformal rapid detection of pesticide residues from fruits. *Sens. Actuators B Chem.* **2017**, *241*, 577–583. [CrossRef]
105. Okeke, E.S.; Huang, B.; Mao, G.H.; Chen, Y.; Zeng, Z.J.; Qian, X.; Wu, X.Y.; Feng, W.W. Review of the environmental occurrence/analytical techniques, degradation and toxicity of TBBPA and its derivatives. *Environ. Res.* **2022**, *206*, 112594. [CrossRef]
106. Zhang, W.H.; Yeo, B.S.; Schmid, T.; Zenobi, R. Single molecule tip-enhanced Raman spectroscopy with silver tips. *J. Phys. Chem. C* **2007**, *111*, 1733–1738. [CrossRef]
107. Zhang, R.; Zhang, Y.; Dong, Z.C.; Jiang, S.; Zhang, C.; Chen, L.G.; Zhang, L.; Liao, Y.; Aizpurua, J.; Luo, Y.; et al. Chemical mapping of a single molecule by plasmon-enhanced Raman scattering. *Nature* **2013**, *498*, 82–86. [CrossRef] [PubMed]
108. Schmid, T.; Opilik, L.; Blum, C.; Zenobi, R. Nanoscale Chemical Imaging Using Tip-Enhanced Raman Spectroscopy: A Critical Review. *Angew. Chem. Int. Ed.* **2013**, *52*, 5940–5954. [CrossRef] [PubMed]
109. Deckert-Gaudig, T.; Taguchi, A.; Kawata, S.; Deckert, V. Tip-enhanced Raman spectroscopy—From early developments to recent advances. *Chem. Soc. Rev.* **2017**, *46*, 4077–4110. [CrossRef] [PubMed]
110. Shao, F.; Zenobi, R. Tip-enhanced Raman spectroscopy: Principles, practice, and applications to nanospectroscopic imaging of 2D materials. *Anal. Bioanal. Chem.* **2019**, *411*, 37–61. [CrossRef] [PubMed]
111. Kim, S.; Yu, N.; Ma, X.; Zhu, Y.; Liu, Q.; Liu, M.; Yan, R. High external-efficiency nanofocusing for lens-free near-field optical nanoscopy. *Nat. Photonics* **2019**, *13*, 636–643. [CrossRef]
112. Brown, L.V.; Zhao, K.; King, N.; Sobhani, H.; Nordlander, P.; Halas, N.J. Surface-Enhanced Infrared Absorption Using Individual Cross Antennas Tailored to Chemical Moieties. *J. Am. Chem. Soc.* **2013**, *135*, 3688–3695. [CrossRef]
113. Meo, V.D.; Crescitelli, A.; Moccia, M.; Sandomenico, A.; Cusano, A.M.; Portaccio, M.; Lepore, M.; Galdi, V.; Esposito, E. Pixeled metasurface for multiwavelength detection of vitamin D. *Nanophotonics* **2020**, *9*, 3921–3930. [CrossRef]
114. Wang, C.; Zhang, Q.; Song, Y.; Chou, S.Y. Plasmonic Bar-Coupled Dots-on-Pillar Cavity Antenna with Dual Resonances for Infrared Absorption and Sensing: Performance and Nanoimprint Fabrication. *ACS Nano* **2014**, *8*, 2618–2624. [CrossRef]
115. Hu, H.; Yang, X.; Zhai, F.; Hu, D.; Liu, R.; Liu, K.; Sun, Z.; Dai, Q. Far-field nanoscale infrared spectroscopy of vibrational fingerprints of molecules with graphene plasmons. *Nat. Commun.* **2016**, *7*, 12334. [CrossRef] [PubMed]
116. Rodrigo, D.; Limaj, O.; Janner, D.; Etezadi, D.; García de Abajo, F.J.; Pruneri, V.; Altug, H. Mid-infrared plasmonic biosensing with graphene. *Science* **2015**, *349*, 165. [CrossRef] [PubMed]
117. Chou, S.Y.; Li, W.-D. Structures for Enhancement of Local Electric Field, Light Absorption, Light Radiation, Material Detection and Methods for Making and Using of the Same. 9182338, 2011.
118. Zhou, L.; Ding, F.; Chen, H.; Ding, W.; Zhang, W.; Chou, S.Y. Enhancement of Immunoassay's Fluorescence and Detection Sensitivity Using Three-Dimensional Plasmonic Nano-Antenna-Dots Array. *Anal. Chem.* **2012**, *84*, 4489–4495. [CrossRef]
119. Zang, F.; Su, Z.; Zhou, L.; Konduru, K.; Kaplan, G.; Chou, S.Y. Ultrasensitive Ebola Virus Antigen Sensing via 3D Nanoantenna Arrays. *Adv. Mater.* **2019**, *31*, 1902331. [CrossRef]
120. Zijlstra, P.; Paulo, P.M.R.; Orrit, M. Optical detection of single non-absorbing molecules using the surface plasmon resonance of a gold nanorod. *Nat. Nanotechnol.* **2012**, *7*, 379–382. [CrossRef]
121. Al Balushi, A.A.; Gordon, R. A Label-Free Untethered Approach to Single-Molecule Protein Binding Kinetics. *Nano Lett.* **2014**, *14*, 5787–5791. [CrossRef] [PubMed]
122. Al Balushi, A.A.; Gordon, R. Label-Free Free-Solution Single-Molecule Protein Small Molecule Interaction Observed by Double-Nanohole Plasmonic Trapping. *ACS Photonics* **2014**, *1*, 389–393. [CrossRef]
123. Haes, A.J.; Haynes, C.L.; McFarland, A.D.; Schatz, G.C.; Van Duyne, R.R.; Zou, S.L. Plasmonic materials for surface-enhanced sensing and spectroscopy. *MRS Bull.* **2005**, *30*, 368–375. [CrossRef]
124. Dantham, V.R.; Holler, S.; Barbre, C.; Keng, D.; Kolchenko, V.; Arnold, S. Label-Free Detection of Single Protein Using a Nanoplasmonic-Photonic Hybrid Microcavity. *Nano Lett.* **2013**, *13*, 3347–3351. [CrossRef]
125. Bozzola, A.; Perotto, S.; De Angelis, F. Hybrid plasmonic-photonic whispering gallery mode resonators for sensing: A critical review. *Analyst* **2017**, *142*, 883–898. [CrossRef] [PubMed]
126. Liang, F.; Guo, Y.; Hou, S.; Quan, Q. Photonic-plasmonic hybrid single-molecule nanosensor measures the effect of fluorescent labels on DNA-protein dynamics. *Sci. Adv.* **2017**, *3*, 1602991. [CrossRef] [PubMed]
127. Al Balushi, A.A.; Zehtabi-Oskuie, A.; Gordon, R. Observing single protein binding by optical transmission through a double nanohole aperture in a metal film. *Biomed. Opt. Express* **2013**, *4*, 1504–1511. [CrossRef] [PubMed]
128. Al Balushi, A.A.; Kotnala, A.; Wheaton, S.; Gelfand, R.M.; Rajashekara, Y.; Gordon, R. Label-free free-solution nanoaperture optical tweezers for single molecule protein studies. *Analyst* **2015**, *140*, 4760–4778. [CrossRef] [PubMed]
129. Yoo, D.; Gurunatha, K.L.; Choi, H.-K.; Mohr, D.A.; Ertsgaard, C.T.; Gordon, R.; Oh, S.-H. Low-Power Optical Trapping of Nanoparticles and Proteins with Resonant Coaxial Nanoaperture Using 10 nm Gap. *Nano Lett.* **2018**, *18*, 3637–3642. [CrossRef]
130. Ye, W.; Celiksoy, S.; Jakab, A.; Khmelinskaia, A.; Heermann, T.; Raso, A.; Wegner, S.V.; Rivas, G.; Schwille, P.; Ahijado-Guzman, R.; et al. Plasmonic Nanosensors Reveal a Height Dependence of MinDE Protein Oscillations on Membrane Features. *J. Am. Chem. Soc.* **2018**, *140*, 17901–17906. [CrossRef] [PubMed]

131. Rosman, C.; Pierrat, S.; Henkel, A.; Tarantola, M.; Schneider, D.; Sunnick, E.; Janshoff, A.; Soennichsen, C. A New Approach to Assess Gold Nanoparticle Uptake by Mammalian Cells: Combining Optical Dark-Field and Transmission Electron Microscopy. *Small* **2012**, *8*, 3683–3690. [CrossRef]
132. Arcadio, F.; Marzano, C.; Del Prete, D.; Zeni, L.; Cennamo, N. Analysis of Plasmonic Sensors Performance Realized by Exploiting Different UV-Cured Optical Adhesives Combined with Plastic Optical Fibers. *Sensors* **2023**, *23*, 6182. [CrossRef]
133. Principe, M.; Consales, M.; Micco, A.; Crescitelli, A.; Castaldi, G.; Esposito, E.; La Ferrara, V.; Cutolo, A.; Galdi, V.; Cusano, A. Optical fiber meta-tips. *Light Sci. Appl.* **2017**, *6*, e16226. [CrossRef]
134. Martínez-Hernández, M.E.; Rivero, P.J.; Goicoechea, J.; Arregui, F.J. Trends in the Implementation of Advanced Plasmonic Materials in Optical Fiber Sensors (2010–2020). *Chemosensors* **2021**, *9*, 64. [CrossRef]
135. Chiavaioli, F.; Santano Rivero, D.; Del Villar, I.; Socorro-Leránoz, A.B.; Zhang, X.; Li, K.; Santamaría, E.; Fernández-Irigoyen, J.; Baldini, F.; van den Hove, D.L.A.; et al. Ultrahigh Sensitive Detection of Tau Protein as Alzheimer's Biomarker via Microfluidics and Nanofunctionalized Optical Fiber Sensors. *Adv. Photonics Res.* **2022**, *3*, 2200044. [CrossRef]
136. Choudhary, S.; Esposito, F.; Sansone, L.; Giordano, M.; Campopiano, S.; Iadicicco, A. Lossy Mode Resonance Sensors in Uncoated Optical Fiber. *IEEE Sens. J.* **2023**, *23*, 15607–15613. [CrossRef]
137. Del Villar, I.; Arregui, F.J.; Zamarreño, C.R.; Corres, J.M.; Bariain, C.; Goicoechea, J.; Elosua, C.; Hernaez, M.; Rivero, P.J.; Socorro, A.B.; et al. Optical sensors based on lossy-mode resonances. *Sens. Actuators B* **2017**, *240*, 174–185. [CrossRef]
138. Pituła, E.; Janik, M.; Sezemsky, P.; Szymańska, K.P.; Olszewski, M.; Stranak, V.; Koba, M.; Śmietana, M. Smartphone-based dynamic measurements of electro-optically modulated lossy-mode resonance and its biosensing applications. *Measurement* **2023**, *206*, 112349. [CrossRef]
139. Karas, M.; Hillenkamp, F. Laser desorption ionization of proteins with molecular masses exceeding 10,000 daltons. *Anal. Chem.* **1988**, *60*, 2299–2301. [CrossRef] [PubMed]
140. Karas, M.; Kruger, R. Ion formation in MALDI: The cluster ionization mechanism. *Chem. Rev.* **2000**, *103*, 427–439. [CrossRef]
141. Chiang, C.K.; Chen, W.T.; Chang, H.T. Nanoparticle-based mass spectrometry for the analysis of biomolecules. *Chem. Soc. Rev.* **2011**, *40*, 1269–1281. [CrossRef]
142. Sekula, J.; Niziol, J.; Rode, W.; Ruman, T. Gold nanoparticle-enhanced target (AuNPET) as universal solution for laser desorption/ionization mass spectrometry analysis and imaging of low molecular weight compounds. *Anal. Chim. Acta* **2015**, *875*, 61–72. [CrossRef]
143. Hinman, S.S.; Chen, C.Y.; Duan, J.C.; Cheng, Q. Calcinated gold nanoparticle arrays for on-chip, multiplexed and matrix-free mass spectrometric analysis of peptides and small molecules. *Nanoscale* **2016**, *8*, 1665–1675. [CrossRef]
144. Zarei, M. Advances in point-of-care technologies for molecular diagnostics. *Biosens. Bioelectron.* **2017**, *98*, 494–506. [CrossRef]
145. Zarei, M. Portable biosensing devices for point-of-care diagnostics: Recent developments and applications. *TrAC Trends Anal. Chem.* **2017**, *91*, 26–41. [CrossRef]
146. Quesada-Gonzalez, D.; Merkoci, A. Mobile phone-based biosensing: An emerging "diagnostic and communication" technology. *Biosens. Bioelectron.* **2017**, *92*, 549–562. [CrossRef] [PubMed]
147. Gao, X.; Wu, N. Smartphone-Based Sensors. *Electrochem. Soc. Interface* **2016**, *25*, 79–81. [CrossRef]
148. Preechaburana, P.; Gonzalez, M.C.; Suska, A.; Filippini, D. Surface Plasmon Resonance Chemical Sensing on Cell Phones. *Angew. Chem. Int. Ed.* **2012**, *51*, 11585–11588. [CrossRef]
149. Min, S.Y.; Li, S.J.; Zhu, Z.Y.; Liu, Y.; Liang, C.W.; Cai, J.X.; Han, F.; Li, Y.Y.; Cai, W.S.; Cheng, X.; et al. Ultrasensitive Molecular Detection by Imaging of Centimeter-Scale Metasurfaces with a Deterministic Gradient Geometry. *Adv. Mater.* **2021**, *33*, 2100270. [CrossRef] [PubMed]
150. Bian, J.; Xing, X.; Zhou, S.; Man, Z.; Lu, Z.; Zhang, W. Patterned plasmonic gradient for high-precision biosensing using smartphone reader. *Nanoscale* **2019**, *11*, 12471–12476. [CrossRef]
151. Nordén, B.; Rodger, A.; Dafforn, T. *Linear Dichroism and Circular Dichroism: A Textbook on Polarized-Light Spectroscopy*; Royal Society of Chemistry: London, UK, 2010.
152. Chen, P.; Ge, S.J.; Ma, L.L.; Hu, W.; Chigrinov, V.; Lu, Y.Q. Generation of Equal-Energy Orbital Angular Momentum Beams via Photopatterned Liquid Crystals. *Phys. Rev. Appl.* **2016**, *5*, 044009. [CrossRef]
153. Song, J.; Zhou, J.; Duan, H. Self-Assembled Plasmonic Vesicles of SERS-Encoded Amphiphilic Gold Nanoparticles for Cancer Cell Targeting and Traceable Intracellular Drug Delivery. *J. Am. Chem. Soc.* **2012**, *134*, 13458–13469. [CrossRef]
154. Radziuk, D.; Moehwald, H. Prospects for plasmonic hot spots in single molecule SERS towards the chemical imaging of live cells. *Phys. Chem. Chem. Phys.* **2015**, *17*, 21072–21093. [CrossRef]
155. Austin, L.A.; Kang, B.; El-Sayed, M.A. Probing molecular cell event dynamics at the single-cell level with targeted plasmonic gold nanoparticles: A review. *Nano Today* **2015**, *10*, 542–558. [CrossRef]
156. Yuan, H.; Register, J.K.; Wang, H.-N.; Fales, A.M.; Liu, Y.; Vo-Dinh, T. Plasmonic nanoprobes for intracellular sensing and imaging. *Anal. Bioanal. Chem.* **2013**, *405*, 6165–6180. [CrossRef] [PubMed]
157. Kumar, S.; Harrison, N.; Richards-Kortum, R.; Sokolov, K. Plasmonic Nanosensors for Imaging Intracellular Biomarkers in Live Cells. *Nano Lett.* **2007**, *7*, 1338–1343. [CrossRef] [PubMed]
158. Wang, W.; Foley, K.; Shan, X.; Wang, S.; Eaton, S.; Nagaraj, V.J.; Wiktor, P.; Patel, U.; Tao, N. Single cells and intracellular processes studied by a plasmonic-based electrochemical impedance microscopy. *Nat. Chem.* **2011**, *3*, 249–255. [CrossRef]

159. Sharifi, M.; Attar, F.; Saboury, A.A.; Akhtari, K.; Hooshmand, N.; Hasan, A.; El-Sayed, M.A.; Falahati, M. Plasmonic gold nanoparticles: Optical manipulation, imaging, drug delivery and therapy. *J. Control. Release* **2019**, *311–312*, 170–189. [CrossRef]
160. Kim, M.; Lee, J.-H.; Nam, J.-M. Plasmonic Photothermal Nanoparticles for Biomedical Applications. *Adv. Sci.* **2019**, *6*, 1900471. [CrossRef]
161. Singh, S.K.; Mazumder, S.; Vincy, A.; Hiremath, N.; Kumar, R.; Banerjee, I.; Vankayala, R. Review of Photoresponsive Plasmonic Nanoparticles That Produce Reactive Chemical Species for Photodynamic Therapy of Cancer and Bacterial Infections. *ACS Appl. Nano Mater.* **2023**, *6*, 1508–1521. [CrossRef]
162. Ali, M.R.K.; Wu, Y.; El-Sayed, M.A. Gold-Nanoparticle-Assisted Plasmonic Photothermal Therapy Advances Toward Clinical Application. *J. Phys. Chem. C* **2019**, *123*, 15375–15393. [CrossRef]
163. Huang, W.T.; Chan, M.H.; Chen, X.; Hsiao, M.; Liu, R.S. Theranostic nanobubble encapsulating a plasmon-enhanced upconversion hybrid nanosystem for cancer therapy. *Theranostics* **2020**, *10*, 782–796. [CrossRef]
164. Zhang, Y.; Gu, Y.; He, J.; Thackray, B.D.; Ye, J. Ultrabright gap-enhanced Raman tags for high-speed bioimaging. *Nat. Commun.* **2019**, *10*, 3905. [CrossRef]
165. Khlebtsov, N.G.; Lin, L.; Khlebtsov, B.N.; Ye, J. Gap-enhanced Raman tags: Fabrication, optical properties, and theranostic applications. *Theranostics* **2020**, *10*, 2067–2094. [CrossRef]
166. Mesch, M.; Metzger, B.; Hentschel, M.; Giessen, H. Nonlinear Plasmonic Sensing. *Nano Lett.* **2016**, *16*, 3155–3159. [CrossRef]
167. Lee, C.; Lawrie, B.; Pooser, R.; Lee, K.G.; Rockstuhl, C.; Tame, M. Quantum Plasmonic Sensors. *Chem. Rev.* **2021**, *121*, 4743–4804. [CrossRef] [PubMed]
168. Yu, R.W.; Cox, J.D.; de Abajo, F.J.G. Nonlinear Plasmonic Sensing with Nanographene. *Phys. Rev. Lett.* **2016**, *17*, 123904. [CrossRef] [PubMed]
169. Lee, J.S.; Yoon, S.J.; Rah, H.; Tame, M.; Rockstuhl, C.; Song, S.H.; Lee, C.; Lee, K.G. Quantum plasmonic sensing using single photons. *Opt. Express* **2018**, *26*, 29272–29282. [CrossRef] [PubMed]
170. Dowran, M.; Kumar, A.; Lawrie, B.J.; Pooser, R.C.; Marino, A.M. Quantum-enhanced plasmonic sensing. *Optica* **2018**, *5*, 628–633. [CrossRef]
171. Verma, M.S.; Chandra, M. Nonlinear Plasmonic Sensing for Label-Free and Selective Detection of Mercury at Picomolar Level. *ACS Sens.* **2020**, *5*, 645–649. [CrossRef]